Article



Dynamic self-reinforcement of gene expression determines acquisition of cellular mechanical memory

Christopher C. Price, ^{1,2} Jairaj Mathur, ^{2,3} Joel D. Boerckel, ^{2,4,5} Amit Pathak, ^{2,3,*} and Vivek B. Shenoy ^{1,2,*}

¹Department of Materials Science and Engineering, University of Pennsylvania, Philadelphia, Pennsylvania and ²Center for Engineering Mechanobiology, University of Pennsylvania, Philadelphia, Pennsylvania; ³Department of Mechanical Engineering and Materials Science, Washington University, St. Louis, Missouri; and ⁴Department of Orthopaedic Surgery, Perelman School of Medicine, University of Pennsylvania, Philadelphia, Pennsylvania and ⁵Department of Bioengineering, University of Pennsylvania, Philadelphia, Pennsylvania

ABSTRACT Mechanotransduction describes activation of gene expression by changes in the cell's physical microenvironment. Recent experiments show that mechanotransduction can lead to long-term "mechanical memory," in which cells cultured on stiff substrates for sufficient time (priming phase) maintain altered phenotype after switching to soft substrates (dissipation phase) as compared to unprimed controls. The timescale of memory acquisition and retention is orders of magnitude larger than the timescale of mechanosensitive cellular signaling, and memory retention time changes continuously with priming time. We develop a model that captures these features by accounting for positive reinforcement in mechanical signaling. The sensitivity of reinforcement represents the dynamic transcriptional state of the cell composed of protein lifetimes and three-dimensional chromatin organization. Our model provides a single framework connecting microenvironment mechanical history to cellular outcomes ranging from no memory to terminal differentiation. Predicting cellular memory of environmental changes can help engineer cellular dynamics through changes in culture environments.

SIGNIFICANCE Cellular mechanical memory has been observed across several different cell lines and culture environments, yet there is limited mechanistic understanding to explain key features of this biological phenomenon. Here, we develop a general mathematical framework that produces the unique features of cellular mechanical memory with a limited number of free parameters. Using the same parameter set and experimental units, our model agrees with experimentally observed distributions of memory outcomes across different cultures. Because data on cellular mechanical memory are time consuming to acquire, an improved theoretical understanding will assist cellular engineering efforts that take advantage of the mechanical environment.

INTRODUCTION

Cellular mechanical memory describes how cells acquire and retain information about the mechanical properties of their microenvironment. These extracellular matrix (ECM) properties impact cellular structure, function, and identity (1–3), and recent experiments suggest that this linkage depends on not just this microenvironment but also the accumulated mechanical history experienced by the cell (4–10). The mechanism by which this memory is

developed, maintained, and lost is not yet understood and exhibits several unusual features. First, the timescale at which the cell responds to mechanical changes through signaling (minutes to hours) is an order of magnitude faster than the timescale of memory development and dissipation (days to weeks). This implies that microenvironmental information is rapidly acquired and used by the cell but stored and released much more slowly. Second, the persistence time of the developed mechanical memory ranges continuously from no memory all the way to permanent memory (cell differentiation), simply by varying the microenvironmental history that the cell is exposed to (Fig. 1 a). This strong coupling between the dynamics of memory retention and the dynamics of the stimulus being remem-

bered is not found in common physical systems such as

Submitted July 21, 2021, and accepted for publication October 5, 2021.

*Correspondence: vshenoy@seas.upenn.edu or pathaka@wustl.edu

Christopher C. Price and Jairaj Mathur contributed equally to this work.

Editor: Guy Genin.

https://doi.org/10.1016/j.bpj.2021.10.006

© 2021 Biophysical Society.



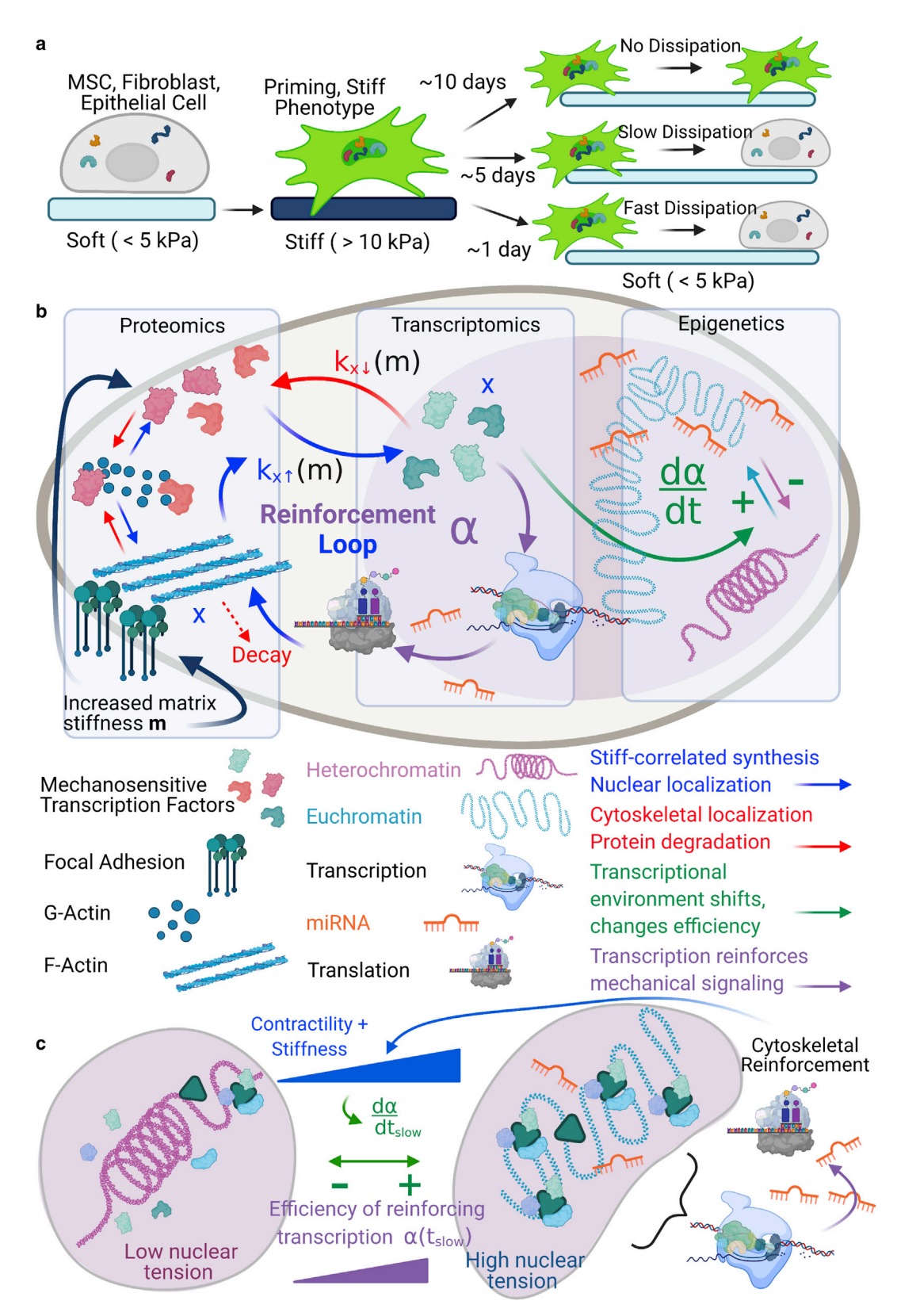


FIGURE 1 Model for dynamic mechanical memory in cells. (a) Experimental observations indicate that cells alter their phenotype when placed on stiff substrates (priming) in a matter of hours. The length of time that these phenotype features are retained when the cell is transitioned backed to soft substrates depends on the length of priming time on the scale of days. (b) Integrated cellular picture of mechanosensitive signaling and positive reinforcement enable by transcription and translation. Increased ECM stiffness leads to F-actin formation, increased cellular contractility, and nuclear localization of mechanosensors

(legend continued on next page)

magnetic or shape memory materials. Understanding these unique dynamical phenomena is critical to engineering cell behavior and fate through temporal control of the cell's physical environment.

Cellular adaptation to changes in the mechanical environment occurs in both the cytoskeletal and nuclear domains (11,12). On stiff substrates, examples of cytoskeletal phenotype changes include increased clustering of focal adhesions, actomyosin contractility, cell spreading area, and migration speed (13–15). On soft substrates, contractility is reduced, and the mechanical properties of the cell adjust to match that of the surrounding environment by depolymerization of F-actin (16-18). In the nucleus, the population of transcriptionally active proteins changes with ECM stiffness as certain transcription factors relocate in response to mechanical signals (19,20). The chromatin structure experiences epigenetic modifications and physical deformation of the nuclear envelope from contractile forces, leading to alterations in gene expression (21,22). The dynamic nature of mechanical memory development and depletion indicates that information about microenvironmental mechanics is continuously consumed by the cell, allowing stem cell differentiation to proceed from different time series of mechanical microenvironments (1,4,6,23).

A hallmark of mathematical models of memory is bistability, which is a property of a system to have more than one steady state, and this concept forms the basis for Waddington's famous landscape of cell differentiation. Bistability alone does not contain any information about dynamics of memory development or retention, only that it can occur (24,25). Several mechanistic models have been put forward to explain the relationship between mechanics and cell differentiation (5,26-28), but these models do not simultaneously capture 1) the timescale disparity between mechanical signaling and cell adaptation and memory development and 2) the continuous range of memory outcomes. More generally, regulatory gene network models with different topologies can give rise to memory using network motifs such as positive and negative reinforcement (29–34). However, explicit molecular network models for mechanotransduction are difficult to develop because there are not enough data available to determine the many model parameters or assert which components of the regulatory network are rate limiting. This leads to rigid models that are difficult to interpret and cannot generalize across variations in priming time and priming stiffness, limiting their predictive power.

In this work, we propose a model to describe the dynamics of mechanotransductive memory acquisition and persistence. The model starts from a general molecular framework, incorporating both fast and slow mechanosensitive pathways. We simplify this model to two ordinary

differential equations, representing cytoskeletal and nuclear dynamics, respectively. First, we show that simple positive reinforcement between signaling and transcription is sufficient for mechanical memory acquisition. Second, we show that dynamic coupling between the cellular phenotype and the sensitivity of this reinforcement leads to a continuous range of memory persistence time. Biologically, the sensitivity of positive reinforcement corresponds to the epigenetic state and transcriptional environment of the cell, which govern the steady-state balance between synthesis and degradation of proteins correlated with either a stiff-ECM or soft-ECM phenotype. The rate at which signaling induces changes in the positive reinforcement sensitivity (transcriptional environment) determines memory by shifting the phenotype (protein composition) from requiring external mechanical signal to a self-sustaining state. Simulating priming programs that match experimentally tested configurations, we observe emergent cases of no memory, temporary memory, and quasipermanent memory (differentiation) by varying only the priming time and keeping other model parameters fixed. In designing future experiments or therapeutics, this simple but robust framework could help decouple the importance of positive reinforcement of mechanosensitive gene expression and their sensitivity to mechanical cues, thus optimizing the role of mechanical memory in optimizing biological outcomes.

MATERIALS AND METHODS

Model for dynamic mechanosensitivity in the cytoskeleton and the nucleus

We begin our model of mechanotransduction and mechanosensitive gene expression by introducing a variable x, which represents the average functional concentration of all the stiff-activated proteins and transcription factors in the cell. Examples of cytoskeletal protein components contributing to x include F-actin (or α -smooth muscle actin (SMA)), vinculin, and integrins. Transcription factors contribute to x through their transcriptionally eligible concentrations, which incorporates nuclear localization as well as cell concentration. Examples of transcription factors with well-known stiff-correlated nuclear localization include YAP (35,36), MKL-1 (20,37), and RUNX2 (38,39). Finally, we include epigenetically modifying enzymes such as HDAC and HAT as contributing components to x, which influence chromatin organization and demonstrate mechanosensitive activity patterns (8). Although these contributing components to x have independent dynamics, we pursue an approximate approach because limited data are available to characterize all the individual interactions between mechanosensitive components. As an average, x measures the net mechanoactivation of the cell induced by increased ECM stiffness. If more information is known about the mechanosensitive dynamics of the individual components of x for a specific cell type, this approach can be generalized as shown in Supporting materials and methods, Section I. The linear dynamics of x can be written as

(blue arrows), whereas soft-ECM stiffness leads to decomposition of these features (red arrows). (c) Slow changes in the stable chromatin state in response to nuclear tension, epigenetic changes, and shifts in the post-transcriptional regulation environment affect the efficiency of stiff phenotype reinforcement. High levels of reinforcement stabilize the stiff phenotype features. To see this figure in color, go online.

$$\frac{dx}{dt} = k_{x\uparrow}(m)(x_{ref} - x) - k_{x\downarrow}(m)x,\tag{1}$$

where m is the matrix stiffness, $k_{x\uparrow}(m)$ gives the mechanosensitive rate of cytoskeletal protein synthesis and/or transcription factor nuclear import, $k_{x\perp}(m)$ gives the rate of the reverse processes (degradation and nuclear export), and x_{ref} is a reference level of mechanoactivation at a characteristic stiffness m_0 . Processes described by $k_{x\uparrow}(m)$ are shown with blue arrows in Fig. 1 b, and processes described by $k_{x\downarrow}(m)$ are shown with red arrows. We choose $k_{x\uparrow}(m)$ to be a monotonically increasing but saturating function of stiffness, $k_{x\uparrow} = \tau_{x\uparrow} - \exp(-\frac{m}{m_0})$, to capture the mechanosensitivity of stiff activation, and for simplicity we choose the degradation and export rate $k_{x\perp}(m)$ to be a constant $\tau_{x\perp}$ over stiffness (36) (Fig. S1). This is motivated by experimental evidence that nuclear import of transcription factors is more mechanosensitive than nuclear export (36) and that cellular response saturates at very high stiffness (40). Although specific functional choices are arbitrary, the results we present are general to different functional forms that maintain a positive correlation of $k_{x\uparrow}$ with stiffness. A systems circuit of our model is included in Fig. S2 for further reference.

Transcription creates positive reinforcement loop for mechanical signaling

Next, we consider that the transcriptional activity of the many individual components of x creates a positive reinforcement loop by enhancing adaptations to increased stiffness of the ECM. For example, YAP and MKL-1 activate transcription of genes that lead to increased stability of focal adhesions, F-actin, and contractility through Rho-Rock pathways and support of G-actin polymerization (41–43). This stabilization releases additional bound cytoplasmic transcription factors to translocate to the nucleus, further increasing x. The transcriptional positive reinforcement is depicted in Fig. 1 b by the purple arrows; we incorporate this positive reinforcement mechanism into Eq. 1 by adding a nonlinear Hill relation:

$$\frac{dx}{dt} = k_{x\uparrow}(m) \left(x_{ref} - x \right) - k_{x\downarrow}(m) x + \alpha \frac{x^{\beta}}{x^{\beta} + 1}$$
 (2)

Here, α is the sensitivity of the positive reinforcement and β determines the sharpness of the Hill function, which transitions from a low value to a high value like a smoothed step function. Positive reinforcement loops in cells have been extensively modeled using Hill relations and are a known source of bistability in dynamical systems (44-46). Bistability indicates at least two steady-state solutions to a dynamical system and underpins hysteresis and memory in many physical systems. Biologically, the sensitivity parameter α contains all the information about the efficiency of the mechanosensitive self-reinforcement, which directly corresponds to the transcription landscape. Like x, we consider α to be an average measure over many components involved in regulating the transcription-translation pipeline, including proteins, messenger RNA (mRNA), noncoding micro RNA (miRNA), and the fraction of heterochromatin/euchromatin in the nucleus. Implicitly, a subset of these α components depend on mechanosensitive components of x and therefore m, coupling cytoskeletal mechanosensing to nuclear activity in our model. Fig. 1 c illustrates how changing α reflects changes in both threedimensional chromatin architecture and post-transcriptional regulation, altering the efficiency of mechanosensitive transcription. In the heterochromatic state, fewer chromatin sites are available for transcription. In the more active euchromatic state, a complex and modifiable regulatory environment (including miRNAs) exists in between the chromatin and downstream protein expression. These transcriptional machinery and regulatory components interact with significant complexity and codependency, and there are insufficient data to parameterize a full microscopic description of these interactions. A generalized derivation for α is given in Supporting materials and methods, Section II, which considers these nonlinear interactions by expanding α as a series expansion of terms weighted to account for cooperativity between regulatory components.

Fast and slow dynamics of transcriptional reinforcement sensitivity

Because x and m have time dependence, we know that α must also have a dynamic evolution $\frac{d\alpha}{dt}$ that is bounded on the fast end by $\frac{dx}{dt}$ and $\frac{dm}{dt}$ because of the underlying dependence of α components on mechanosensitive x components. On the slow end, the dynamics of α can be severely limited by complex rate-limiting or anticooperative relationships between the transcription-translation regulatory components. Evidence of these time-dependent relationships between reinforcement and transcription has been collected on some individual mechanosensitive mechanisms (47,48). Although we lack the data and explicit mechanistic understanding to specify all the contributing mechanisms to α , we can capture the essential nature of this time dependence by rewriting α as the sum of a fast-changing component (on the scale of $\frac{dm}{dt}$ or $\frac{dx}{dt}$) and a slow-changing component that is effectively constant on the timescale of x and x. Complete details of the derivation beginning from the series expansion of α are included in Supporting materials and methods, Section II; the result for $\alpha(t)$ is

$$\alpha(t) = \alpha(t_{slow}) + c \frac{m^{\zeta}}{m^{\zeta} + 1}$$
 (3)

We use another Hill relation in stiffness m with degree ζ and sensitivity c to model the fast portion of α , which captures the fact that the positive reinforcement sensitivity is explicitly mechanosensitive and that stiff reinforcement requires the presence of mechanosensitive transcription factors such as YAP and MKL-1 to occur (41,42,49–51). Recent evidence indicates that the nuclear structure and chromatin conformation physically respond to environmental stiffness via forces transmitted through the linker of nucleoskeleton and cytoskeleton (LINC) complex and not merely through chemical signals, and these direct processes are captured by this fast component of $\alpha(t)$ (12,52,53). For the remaining term $\alpha(t_{slow})$, we choose a form that generally depends on x and m such that $\frac{\partial \alpha}{\partial t_{slow}}(x, m)$ represents a weighted average of the slow, nonlinear dynamics present in transcription-translation reinforcement.

Plugging Eq. 3 back into Eq. 2, our time-dependent equation for cellular mechanoactivation is now

$$\frac{dx}{dt} = k_{x\uparrow}(m) \left(x_{ref} - x \right) - k_{x\downarrow}(m) x
+ \left(\alpha(t_{slow}, x, m) + c \frac{m^{\zeta}}{m^{\zeta} + 1} \right) \frac{x^{\beta}}{x^{\beta} + 1}$$
(4)

In this ordinary differential equation (ODE), we established mechanosensitivity of synthesis and nuclear import of x (first term), mechanosensitivity of degradation and nuclear export of x (second term), and positive reinforcement of cellular mechanoactivation (third term) with a time-dependent sensitivity that evolves slowly with respect to changes in x. Equation 4 is the key ODE that underpins the results. We can interpret this equation as the negative gradient of a "Waddington-like" energy landscape with respect to x; $\frac{dx}{dt} = -\frac{\partial U}{\partial x}$. Because $\alpha(t_{slow}, x, m)$ evolves on a much slower timescale than $\frac{dx}{dt}$, we treat α as a constant when finding the steady-state solutions of x. Integrating Eq. 4, we arrive at

$$U(x, m, \alpha) = -k_{x\uparrow}(m)x_{ref}x + \frac{x^2}{2}(k_{x\uparrow}(m) + k_{x\downarrow}(m))$$
$$+x\left(\alpha + c\frac{m^{\zeta}}{m^{\zeta} + 1}\right)\left({}_{2}F_{1}\left[1, \frac{1}{\beta}, 1 + \frac{1}{\beta}, -x^{\beta}\right] - 1\right), (5)$$

where $_2F_1$ is the special hypergeometric function.

The model was implemented using a standard ODE solver (fsolve) in the open source SciPy package (Python). Parameter selection for numerical simulations was performed using Latin hypercube sampling over the following parameter space: α_0 (initial value for positive reinforcement), m_0 (stiffness normalization constant), x_{ref} (reference level of mechanoactivation), τ_s (timescale for $\frac{d\alpha}{dt}$), $\tau_{x\downarrow}$ (timescale for x decrease), $\tau_{x\uparrow}$ (timescale for x increase), ζ , β (degree of Hill relations), σ (standard deviation of noise), and A (amplitude of noise). Each parameter combination was run for priming times of 3, 7, and 10 days, with 250 noisy trials run for each priming time. Parameter combinations were scored against the experimental data from Yang et al. (6) using a Kolmogorov-Smirnov test, a least-squares test, and manual inspection. We note that these parameter combinations do not represent global best fits to the data but were sufficient to show qualitative agreement and differentiate the two different dynamics approaches.

RESULTS

By taking x and α as average quantities over many interacting mechanosensitive components, our implemented model framework sacrifices some mechanistic detail. However, we successfully identify that nonlinear dependence of the positive reinforcement strength on the level of mechanosensation can lead to all the features of mechanical memory observed in experiments. A mechanistic example of this type of positive reinforcement is given in Fig. 2, with connections to the model components illustrated in Fig. 1. Under a stiff mechanoresponse, focal adhesion, integrin, and stress fiber density all increase (54) from increased F-actin polymerization, freeing transcription factors such as MKL-1, YAP, and HDAC to translocate to the nucleus (8,55). These processes correspond to the mechanosensitive linear dynamics introduced in Eq. 1. Significant cross talk has been observed for these transcription factors, which can lead to nonlinear dynamics (56) such as those introduced in Eq. 3. MKL-1 acts as a transcription factor for the production of miR-21 (5), which was found to regulate mechanical memory. miR-21 has also been shown to affect YAP via RUNX1 and RUNX2, which are also mechanosensitive transcription factors (57). Finally, YAP has been shown to regulate actin dynamics, stabilizing F-actin through the Rho pathway (58) and closing the positive reinforcement loop. These processes are examples of fast-acting positive reinforcement; meanwhile, epigenetic modifiers can lead to slow dynamics of chromatin conformational change (59,60). Although this is not a complete account of mechanotransductive pathways by any means, this illustrates one example of mechanically initiated positive reinforcement that couples the cytoskeleton and nucleus and can lead to memory.

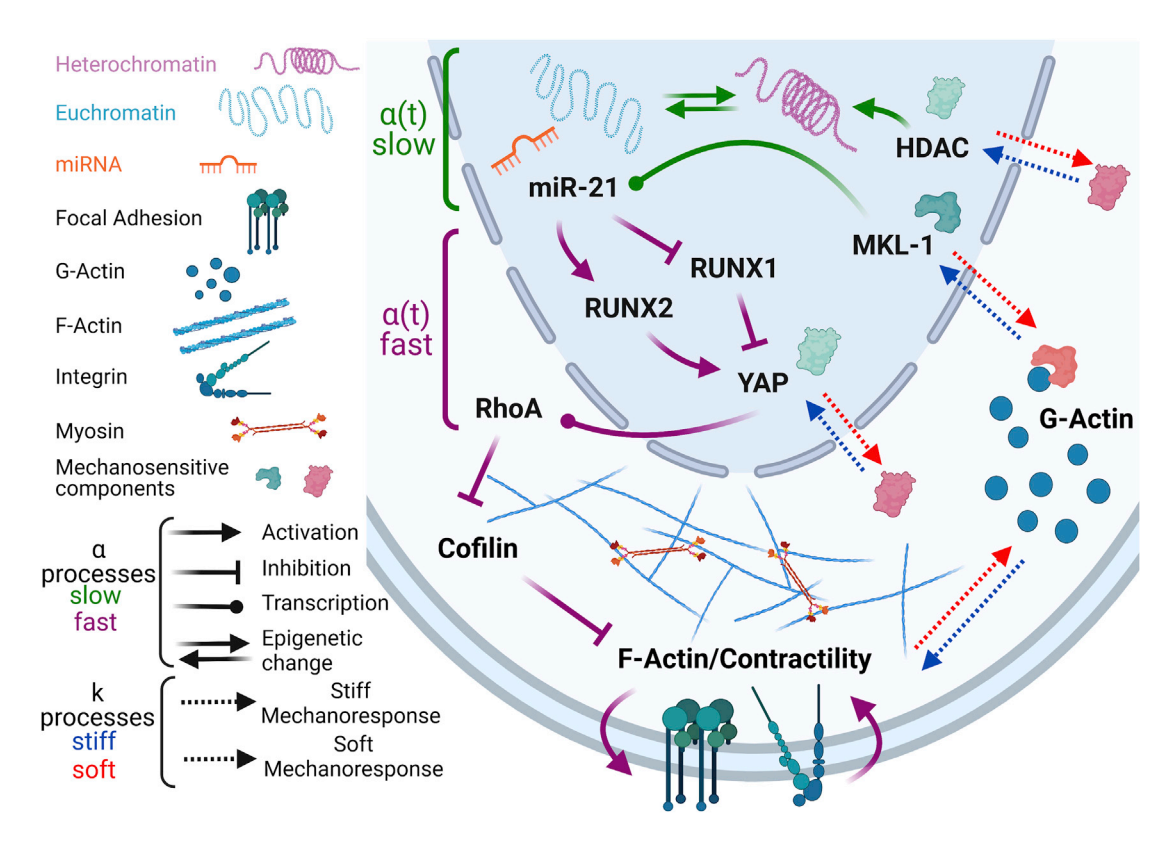


FIGURE 2 Example microscopic mechanosensitive positive reinforcement loop. Relationships assembled from the literature illustrate one example of a positive reinforcement loop in mechanotransduction mediated by transcription factors. In the model, the stiff mechanoresponse corresponds to larger x, and the soft mechanoresponse corresponds to smaller x. The degree of positive reinforcement is controlled by the intensity and magnitude of the activation, inhibition, and transcription arrows, which is captured by α in the model and exhibits both fast and slow dynamics. To see this figure in color, go online.

Phase diagram of cellular mechanoactivation shows selective bistability

We can visualize the steady-state solution space of x through the lens of the energy landscape defined by Eq. 5. Fig. 3 a gives a phase diagram with three distinct regions of the solutions of x (identified as local minima in the free energy landscape) as a function of the dimensionless ECM stiffness $\frac{m}{m_0}$ (y axis) and the reinforcement sensitivity α (x axis). The insets on the phase diagram show representative slices of the energy landscape for a point (α, m) within each region of the landscape.

In orange region I (low reinforcement sensitivity and stiffness), the energy minimum and single corresponding steady state are found at small x. In this monostable region, there is low mechanical signal from the soft ECM, and low α

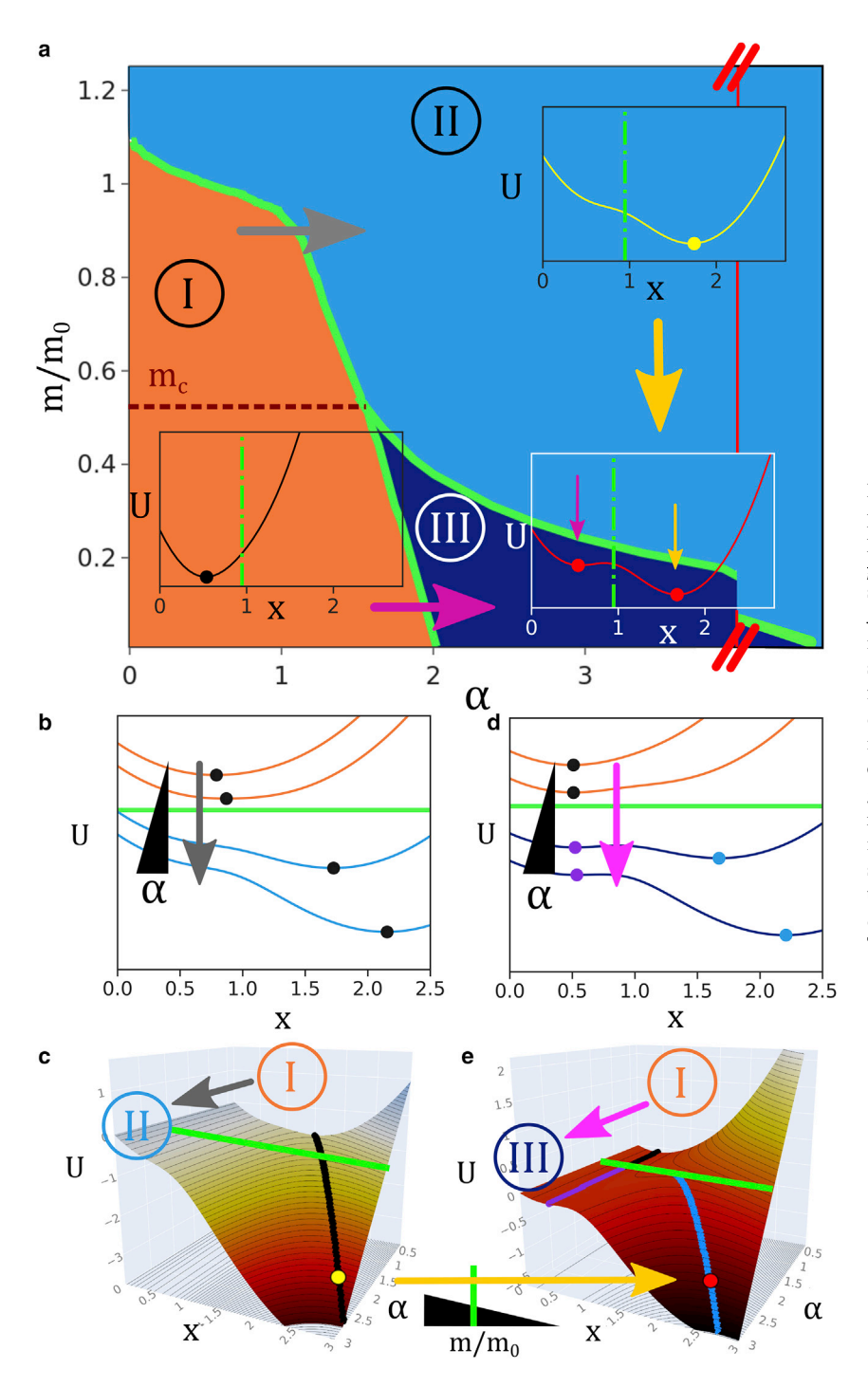


FIGURE 3 Phase diagram of the stiff-correlated phenotype. (a) Phase diagram of steady-state stiff phenotype expression in the space of ECM stiffness $\frac{m}{m_0}$ and transcriptional reinforcement sensitivity α . Insets demonstrate a slice of the energy surface versus x for a typical point in each region, where the dots mark the energy minima and the corresponding steady-state values of x. (b and c) Transitioning from region I to region II (gray arrows) by increasing α at constant stiffness above m_c leads to a significant increase in the steady-state value of x. Green line indicates crossing the phase boundary between regions. (d and e) Transitioning from region I to region III (pink arrows) at constant stiffness by increasing α below m_c traps the system in a low-x steady state. However, the transition from region II to region III by dropping the ECM stiffness at large α (gold arrows) keeps the system in a high-x minima. To see this figure in color, go online.

corresponds to a small influence of the positive reinforcement process on x. In light blue region II, the system is still monostable, but the increased ECM stiffness induces mechanical signaling and shifts the steady-state value of x to a much higher value than in region I. Biologically, this corresponds to mechanotransductive responses that occur on a timescale of hours, such as polymerization of G-actin to F-actin and increased density of focal adhesions, stress fibers, and integrins. Compared to region I, a cell in region II exhibits greater nuclear localization of transcription factors such as YAP, RUNX2, and MKL-1 and increased focal adhesions, contractility, and areal spreading (Fig. 1 b). When $m >> m_0$, this mechanically induced phenotype shift occurs for all values of reinforcement α . In dark blue region III (low stiffness and large reinforcement sensitivity), the system is bistable; there are two steady states for x, one corresponding to a soft phenotype (expected because of the ECM stiffness) and one corresponding to a stiff phenotype (stabilized by the positive reinforcement even without direct mechanical signal). For a given value of ECM stiffness and reinforcement sensitivity in region III, the cell will exhibit either low or high mechanoactivation contingent on the prior mechanical history and the gene expression environment. This hysteresis forms the basis in this framework for cellular mechanical memory.

Dynamically, region boundaries (green lines) in the phase diagram can be crossed by altering either the ECM stiffness or the reinforcement feedback sensitivity, inducing transitions in the steady-state mechanoactivation. Considering the soft phenotype region I as the initial condition, there are two possible transition pathways. Traversing to region II by increasing α above a critical stiffness (gray arrow) leads to a continuous and reversible increase in the observed value of x (Fig. 3, b and c). If the mechanical signal is then removed (region II to region III, gold arrow), x will remain elevated as the minimum from region II smoothly transitions to the large x minima in region III (Fig. 3, c and e). Traversing from region I to region III below the critical stiffness value (pink arrow, Fig. 3 d) will not observably change x from the low region I value, as the region I minimum smoothly transitions to the small x local minimum in region III (Fig. 3 e). Further increasing the positive reinforcement sensitivity within region III eventually leads back to region II, with a single "stiff" steady state at large x for all values of ECM stiffness. The hysteresis loop created by the path dependence in the stiffness-reinforcement phase diagram provides a mechanism for dynamic mechanosensitive memory. A key feature of the phase diagram that corresponds to experimental observations is that increasing mechanical stiffness alone can increase x, allowing the cell to begin adapting to the environment on short timescales by expressing stiff-correlated proteins and localizing stiff-correlated transcription factors to the nucleus (1). However, these changes are fully reversible (exhibit no memory) unless the sensitivity of the positive reinforcement is sufficiently large. In the next section, we explore how evolving α on a slow timescale can lead to different expressions of mechanical memory depending on the time program of external mechanical stimulus.

Nonlinear dynamics of positive reinforcement sensitivity capture full range of memory retention outcomes

Having shown that the trajectory of α can determine whether memory is observed for a particular ECM mechanical history, we return to $\alpha(t_{slow})$ in Eq. 3 and consider an explicit form for the slow evolution of the reinforcement sensitivity. Given sufficient data on low-level biological dynamics, $\alpha(t_{slow})$ can be rigorously derived from Eq. S3 (Supporting materials and methods, Section II), but in lieu of these data, we choose the following form to maximize simplicity while capturing key phenomenological features from experiment:

$$\frac{d\alpha}{dt_{slow}} = \begin{cases}
-\frac{\alpha - \alpha_0}{\tau_f}, & I \\
\frac{\alpha}{\tau_s} \frac{m}{m_0} \exp{-\frac{x}{x_{ref}}}, & II \\
-\frac{\alpha}{\tau_s} \frac{m_0}{m} \exp{-\frac{x}{x_{ref}}}, & III
\end{cases} (6)$$

where τ_f and τ_s are time constants on the scale of hours and days, respectively, and can be directly related to $\frac{dy_i}{dt}$ and $\frac{dz}{dt}$ in Eq. S4. Fig. 4 overlays the biological interpretations of the different piecewise components of Eq. 6 on top of the phase diagram from Fig. 3 a. The y axis remains the rescaled ECM stiffness m/m_0 and the x axis the strength of positive mechanosensitive reinforcement α .

In region I (low stiffness and cytoskeletal reinforcement), we simply set $\frac{d\alpha}{dt_{stow}}$ to quickly converge to a reference value α_0 . At low levels of mechanical signaling and without prior mechanical activation, there is no driving force to spur phenotypic change. Although soft ECMs promote cell differentiation and memory, in our example we are only considering stiff-correlated genes for x, and there is no evidence for undifferentiated cells to develop memory that resists stiff priming. In Fig. 4, this corresponds to no change in the chromatin state or transcriptional activity over time. Memory develops at high stiffness and is lost at low stiffness unless the cell differentiates, so we choose α to increase in region II and decrease in region III to complete our piecewise description. By our definition, increasing $\alpha(t_{slow})$ in region II accounts for slow, nonlinear processes (shifts in the three-dimensional chromatin and transcriptional regulation environment) that increase reinforcement of a stiff cellular phenotype (Fig. 4). Decreasing $\alpha(t_{slow})$ in region III models net decay of these stiff phenotype features (which can have lifetimes on the scale of days to weeks (61)) and reversal of

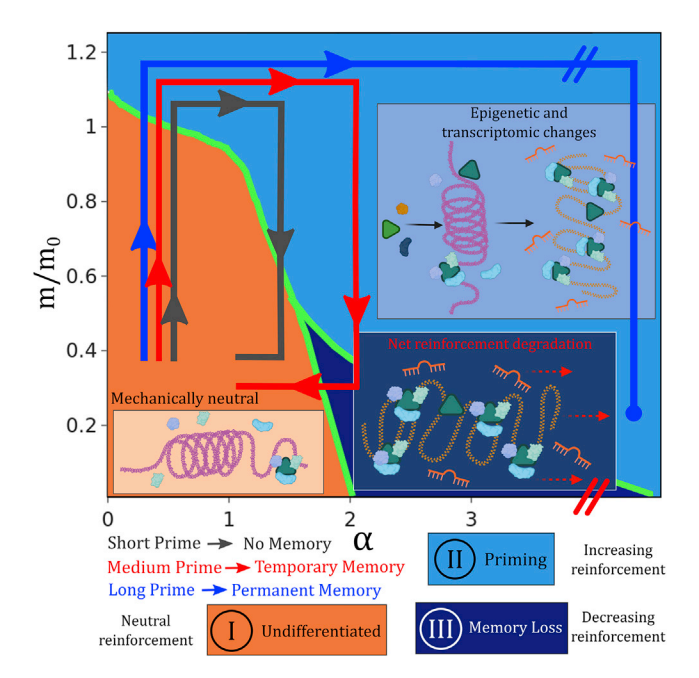


FIGURE 4 Dynamics of the transcriptional environment. In region I, the cell receives little mechanical signal and has limited positive reinforcement, so there is no driving force for the transcriptional environment to shift. In region II, signaling is sufficient to drive chromatin reorganization and changes to the post-transcriptional regulatory environment, such as miRNA synthesis. In region III, the mechanical signal is lost, and there is net degradation and reversal of the stiff-correlated phenotype. As self-reinforcement α increases, less external mechanical signal is required to maintain the stiff phenotype cultivated in region II. To see this figure in color, go online.

the transcriptional environment in the absence of sufficient mechanical signal.

In the priming region II, multiplying by $\frac{m}{m_0}$ ensures that the priming time required to achieve a given level of memory decreases when increasing the priming stiffness. Including a dependence on x ensures that the persistence time of mechanical memory increases nonlinearly with priming time for a specified priming stiffness (6). Mechanistically, our definition of x includes mechanosensitive epigenetic modifiers such as HDAC and HAT (8,62,63), and although the activity of these enzymes to flip epigenetic marks occurs on shorter timescales relative to memory (62), chromatin structural organization and downstream effects on transcription can be much slower because of the glassy dynamics of actual chromatin conformational change (59,60,64). This couples the slow dynamics of the reinforcement sensitivity to the steady-state value of x, which changes depending on the specific location within each region of the phase diagram. To our knowledge, this coupling of reinforcement sensitivity to the signal itself is a new feature of our model that has not been studied in other models of cellular positive reinforcement loops. For simplicity and to limit free parameters, we choose the α degradation dynamics in region III to be the reverse of the priming dynamics. Net degradation of the reinforcement and dissipation of memory will be faster at smaller m and will smoothly change from the value of α in region II.

Each of the three arrows (gray, red, and blue) in Fig. 4 correspond to a different hypothetical stiff-priming program that leads to a different class of memory outcome. The initial conditions, priming stiffness, and model parameters (Table 1) are fixed across the three programs. The corresponding time evolution of x and α for each mechanical priming program is plotted in Fig. 5, a-c. Between each of the three priming program results shown in Fig. 5, a-c, only the length of time that the simulated cell is exposed to stiff substrate (10 kPa) is changed; the soft substrate is modeled at 2 kPa.

Short priming does not lead to memory formation

The gray program does not exhibit any memory; the time that the cell is exposed to the stiff environment is short, and when the cell is returned to a soft ECM, the system returns to region I. Although the phenotype quickly shifts to respond to the stiffening substrate at the beginning of the priming program (crossing the dashed green line corresponding to the boundary between regions I and II), the mechanical signal is not maintained long enough to alter the transcriptional environment to the point where it can sustain memory. The stiff phenotype is lost just as rapidly as it was gained (timescale of hours), as the dynamic trajectory returns directly to region I when the stiffness is relaxed. In the case of a stem cell, this corresponds to an insufficient mechanical signal to sustain differentiation.

Medium priming leads to temporary memory with variable retention time

The red program in Fig. 4 exhibits temporary memory: by holding the cell in priming region II for longer than the gray program, α increases sufficiently such that when the

TABLE 1 Parameters for simulations.

Parameters (Fig. 5)	Values	Units
Phase diagram		
m_0	6.5	kPa
X_{ref}	2	arbitrary
β	6	n/a
ζ	35	n/a
c	1	h^{-1}
$ au_{x\downarrow}$	1.5	h
$ au_{x\uparrow}$	1.5	h
Dynamics		
$ au_f$	12	h
$ au_{s}$	150	h
α_0	1	arbitrary
Priming		·
m_{stiff}	10	kPa
m_{soft}	2	kPa

Simulations in Fig. 5, *a*–*d*. n/a, not applicable.

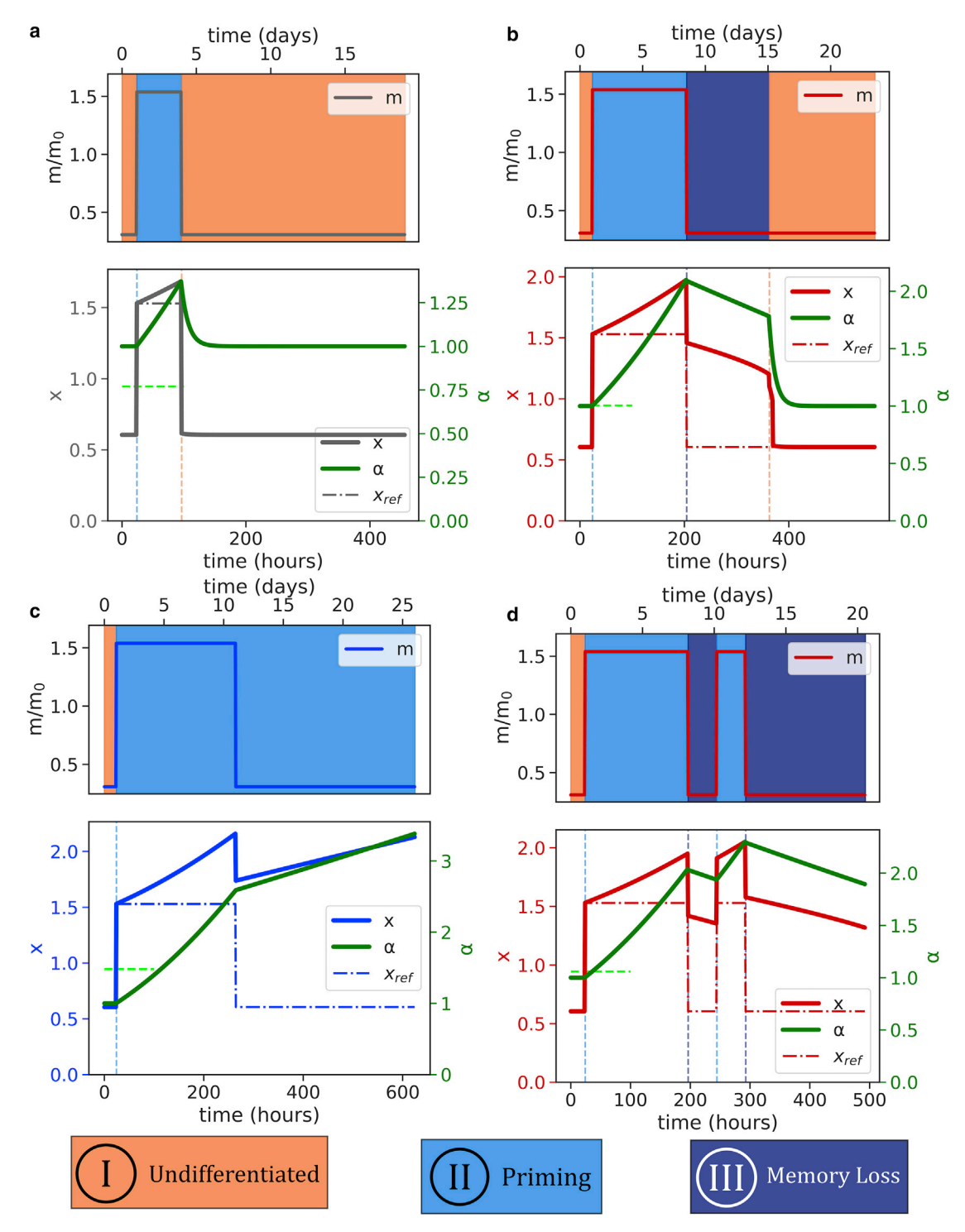


FIGURE 5 Applying different mechanical priming programs. Dot-dash lines x_{ref} indicate the value of x without α dynamics ($\alpha = \alpha_0$). Chart highlight colors indicate phase diagram regions in Fig. 2 and Fig. 3. (a) Short priming time of a few days does not result in memory (gray trajectory in Fig. 3). (b) Medium priming time (red trajectory in Fig. 3) results in memory on the timescale of priming, but eventually this memory decays and the system resets. (c) Longer priming time (blue trajectory in Fig. 3) prevents the system from entering the memory dissipation region when the substrate stiffness is decreased, leading to permanent memory of stiff phenotype. All model parameters in (a)—(c) are fixed except for the length of priming time in the mechanical program (top plots). (d) Two-phase mechanical priming program that illustrates cumulative priming. The first priming phase is identical to (b), and the total priming is equivalent to (c). The second short priming pulse generates significantly more memory than the first priming pulse, yet the cell remains reversibly plastic compared to (c) because some priming decays between the two pulses. To see this figure in color, go online.

cell is returned to a soft environment, it enters the bistable region III. The positive reinforcement loop traps the system in a steady state of large x despite the absence of persisting stiff mechanical signaling (Fig. 5 b). The dot-dash line x_{ref} shows the phenotype expression of x in the absence of α dynamics (α is fixed at α_0) under the same priming program. The significant deviation of x from x_{ref} represents the "phenotypic distance" of the cell from the low reinforcement case; the length of time that this difference is maintained (while the cell is in region III) gives the length of time of observed memory. Because the dynamic evolution of α fundamentally changes the energy surface, the persistence time of memory is decoupled from the relaxation rate of x, as is observed experimentally. Depending on the specific length of priming time and priming stiffness, the model predicts a continuous range of memory persistence times from much shorter than the priming time to much longer than the priming time using the same parameter set. Over time, α slowly decreases (driving x to decrease) because of the absence of continued signaling promoting epigenetic change and natural degradation of stiff phenotype proteins, dissipating memory and eventually returning the system to region I. The model also predicts that as substrate stiffness decreases after priming, the window of reversible memory (range of α that corresponds to region III) grows significantly. This means that the phenotype of the cell is more likely to be reversible if the dissipative mechanical signal is stronger.

Long priming leads to permanent memory

Finally, the blue program corresponds to permanent memory, which in the case of MSCs indicates lineage specification to a stiff phenotype (osteocyte). As the sensitivity of the positive reinforcement α continues to increase, it requires a stronger reversing signal (softer ECM) to enter the bistable, temporary memory regime. At a certain point (beyond the axis break in Fig. 4), it becomes practically impossible to sufficiently reverse the mechanical signaling, and the cell will permanently exhibit a phenotype correlated with large x and saturated large α . In vitro experiments confirm that differentiated osteocytes exhibit sustained higher nuclear activation of YAP/TAZ and other stiff-correlated proteins, qualitatively agreeing with our picture of a phenotype that retains features of high x (50). Fig. 5 c shows how simply increasing the priming time using the same ECM stiffnesses of the mechanical programs in Fig. 5, a and b prevents the system from leaving region II of the phase diagram after the priming phase. Physically, this means that the transcriptional and epigenetic state of the cell has absorbed enough mechanical signal during the priming phase to self-sustain the stiff phenotype once that signal is removed. Even after reducing the ECM stiffness, α and x will continue to slowly increase until they reach a saturation value that corresponds to lineage specification (Fig. S3). The model predicts that this transition to a "permanent" phenotype is a result of the net cumulative mechanical signal absorbed by the cell; for example, consecutive short priming programs will have an additive effect due to the dynamics of α in regions II and III (Fig. 5 d). In this trajectory, the initial priming period is the same as that in Fig. 5 b, but the short second prime ends up building significantly longer memory than in Fig. 5 b because of the accumulated "environmental knowledge," which is not dissipated in the short intermediate soft period. This agrees with experimental evidence that cyclical stretching and stress stiffening of cellular substrates induces stiff differentiation (a "pumping" effect) (23,65,66). The model also predicts that if the epigenetictranscriptional state labeled by α is manipulated by a drug or other mechanism, the cell can lose its permanent mechanical memory and be "reprogrammed," which corresponds physically to reversible lineage specification enabled by so-called Yamanaka factors (67).

Noise in α dynamics results in qualitatively accurate memory distributions when compared with experiment

We have so far identified and predicted a wide range of phenomenological features of cellular mechanical memory with our simple, dynamic positive reinforcement model at the single cell level. However, biological systems are inherently noisy and experimental measurements of cellular phenotype and mechanical memory are most often taken over a population of cells. We categorize possible random fluctuations in our model into two categories: noise that affects mechanosensation and signaling ("fast" noise) and noise that affects the slower dynamics of reinforcement ("slow" noise). "Fast" noise contains all the fluctuations that might cause the phenotype of a cell to not occur at the local minimum of the energy landscape on fast timescales (deviations away from steady state). This is particularly relevant in the bistable region III, where fluctuations could cause cells to jump between different local minima, corresponding to changes in phenotype and changing observations of memory. In a bistable energy landscape, a normal distribution of fluctuations away from steady-state values of x will bias a population toward the global minimum over the local minimum because the jump rate will be higher if the energy barrier height between wells is lower (Fig. S4). Fig. 6 a shows the global minimum steady-state value of x over the stiffness-reinforcement phase diagram from Fig. 3 a (region boundaries in green). In the majority of region III, the high-x minimum is lower in energy. For our purposes of stiff-priming programs that enter region III from a single-minima, high-x state in region II, this means that fluctuations from steady state will tend to reinforce a noisy population to remain in the high-x state, preserving memory and having little qualitative effect on the model results.

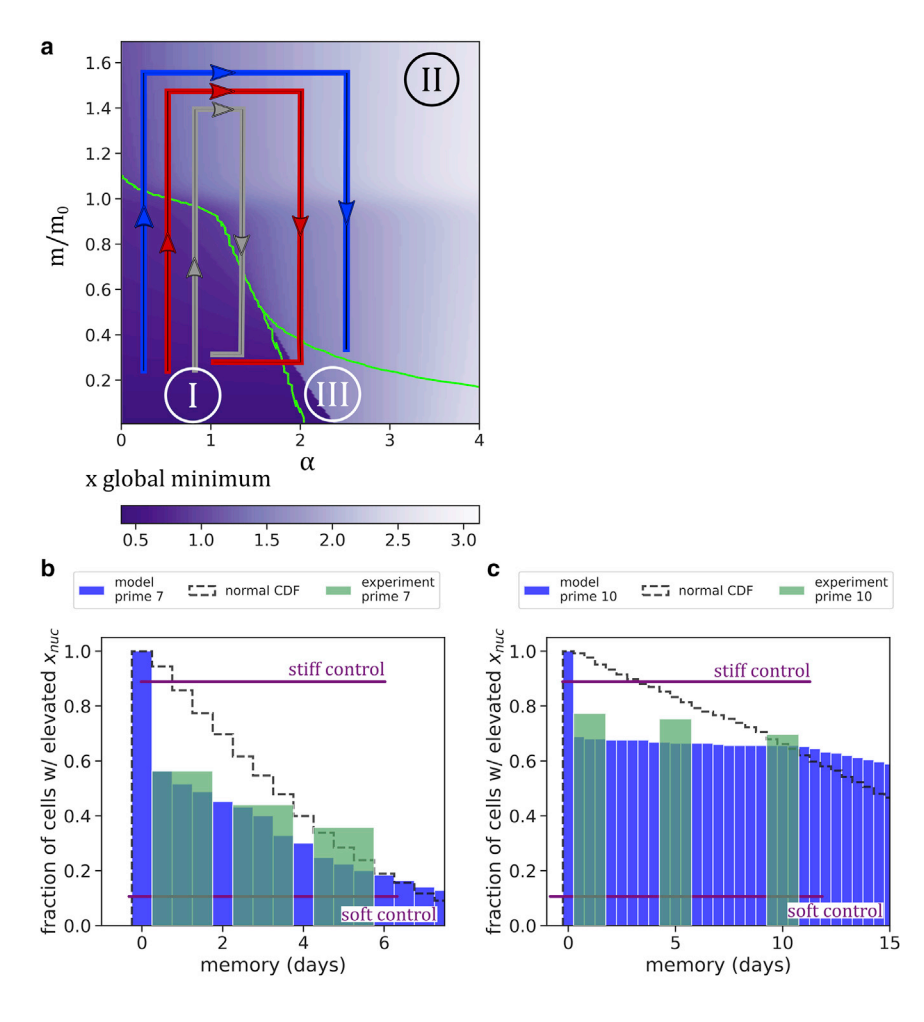


FIGURE 6 Adding noise to nonlinear α dynamics. (a) Global energy minima of x vs. α and m overlaid with priming programs from Fig. 3 and phase boundaries from Fig. 2. For the majority of region III, the large x minima are also the global energy minima, indicating that noise on fast timescales is unlikely to cause well hopping and disrupt temporary memory. (B and C) CDF of memory times from simulations with slow, Gaussian noise incorporated onto $\frac{d\alpha}{dt}$ for priming of 7 days (b) and 10 days (c), matching experimental conditions from Yang et al. (6). Fig. 3 (green bars and purple control lines). The black dashed line shows the CDF of a normal distribution with the same mean and standard deviation as the model distribution for reference. To see this figure in color, go online.

"Slow" noise captures fluctuations in the dynamic evolution of α , and this is more interesting to consider because of the nonlinearity of $\alpha(t)$. The fact that $\frac{d\alpha}{dt}$ depends on the current steady state of x (and therefore the prior history of $\frac{d\alpha}{dt}$) means that a normal distribution of noise in the dynamics of α could lead to a non-normal distribution of memory results. We investigated the impact of including noise on $\frac{d\alpha}{dt}$ by introducing a normal distribution of noise with 0 mean, unit standard deviation, and magnitude A = 0.01 at each time step of the simulations conducted in Fig. 5, a-c and generating a distribution of results over N = 256 simulations. The distribution of memory times observed from the noisy simulations is shown in blue in Fig. 6, b and c. These data contain all simulation runs including those without memory, so the difference between the first bin and second bar shows the percentage of trials (cells) that did not exhibit any mechanical memory. The thin black line gives the cumulative distribution function of a normal distribution with the same mean and standard deviation as our generated data set. This confirms that applying normally distributed noise to the dynamic evolution of α results in a non-normal distribution of observed memory persistence times because of the nonlinearity of the α dynamics.

Experimental data on the persistence time of YAP and RUNX2 nuclear localization as a function of priming time on stiff substrates (10 kPa) taken from (6) are overlaid on Fig. 6, b and c. We averaged their results from YAP and RUNX2 to get a general sense of how the mechanoactivated cell population changes over time (green bars) after the substrate is switched from stiff to soft (2 kPa). The purple control lines indicate the experimental baseline of mechanoactivation in nuclear-localized YAP and RUNX2 without any substrate switching. With added noise, our model captures the qualitative changes in the phenotype distribution over time as priming time is changed, with longer-primed cells being more resistant to return to the soft control phenotype. As in Fig. 5, all parameters aside from priming time are held constant between Fig. 6b and Fig. 6c, replicating experimental conditions (Table 2). In both the experimental data and the model, 10 days of priming leads to significantly higher retention of the stiff phenotype in the cell population than 7 days of priming.

To isolate the effect of the nonlinear coupling between mechanical signaling (x) and transcriptional environment dynamics $\alpha(t)$ on the population statistics, we attempted the same noisy simulations using a linear form for $\frac{d\alpha}{dt_{trans}}$ without

TABLE 2 Parameters for simulations

Parameters (Fig. 6)	Values	Units
Phase diagram		
m_0	6.1	kPa arbitrary
X_{ref}	1.2	
	4.9	n/a
β ζ	35	$rac{n/a}{h^{-1}}$
c	1	
$ au_{x\downarrow}$	1.1	h
$ au_{x\uparrow}$	1.5	h
Dynamics		
$ au_f$	12	h h
$ au_s$	160	
α_0	1	arbitrary
Noise		
σ	0.7	arbitrary
A	0.01	arbitrary
Priming		·
m_{stiff}	10	kPa
m_{soft}	2	kPa

Simulations in Fig. 5, b and c.

x or m dependence (Fig. S5), and did not find the same qualitative agreement. This emphasizes that the nonlinear coupling between mechanical signaling and the dynamic evolution of the transcriptional environment is a fundamental conceptual ingredient that can explain both the disparate timescales of cellular adaptation and memory and capture non-normal population statistics. The linear noise simulations can still result in zero, temporary, or permanent memory. However, the population statistics reflect the normal distribution of the noise applied, as seen by the agreement between the red model results and the black normal cumulative distribution function (CDF). Although the available experimental data are limited, the same set of parameters using linear dynamics cannot qualitatively capture the experimental population distribution change with priming time nearly as well as the nonlinear dynamics, despite the same number of free parameters. The selection procedure for choosing the free parameters is discussed in the Materials and methods.

Model feature comparison with general experimental observations

We selected the data from the Yang et al. study (6) on mesenchymal stem cells for direct comparison with our model because this is one of the few experimental studies to explicitly track components of cellular mechanotransduction as a function of mechanical priming time. Although drawing quantitative comparisons across different experimental studies is difficult because of confounding variables such as cell lineage and growth media, we highlight several features of our model that appear in other studies (results summarized in Table S1). In our model, increasing ECM stiffness enough will always lead to cellular expression of a stiff phenotype on the scale of $\tau_{x\downarrow}$ and $\tau_{x\uparrow}$ irrespective of memory formation; our chosen values for these parameters are based on the adaptation

time observed experimentally of $\sim 1 \text{ h}$ (17). The characteristic stiffness value m_0 that we use in Figs. 5 and 6 is consistent with the priming and memory stiffnesses used in other experiments in Table S1. A short priming of ~ 1 day does not lead to appreciable memory in both our model and experiments (7), and temporary memory retention time is generally greater than or equal to the priming time across different experiments. In our phase diagram, reduction of α from region II to region III or region I erases permanent memory; experimentally, knockdown of miR-21 (a component of $\alpha(t_{slow})$) also erased permanent memory even after long priming (5). Temporary memory development correlated with RUNX2 nuclear localization using stiff and soft substrates of 8 and 0.5 kPa after 7 days of priming was recently observed by Watson et al. in epithelial cells (9); these values are similar to the data from Yang et al. (6), indicating that similar parameters in our model are translatable to a different cell type. Finally, in our model the reinforcement strength and acquired memory are cumulative; this agrees qualitatively with experiments that have investigated dynamic cyclical stretching as a way to observe mechanical memory (23,66). Fig. 7, a-c gives a schematic overview of the progression from external mechanical signal to self-sustaining mechanical memory with increased priming time by way of increased transcriptional reinforcement, spurred by mechanotransduction.

Simple generalization for analogous soft-ECM correlated mechanical memory

In this work, we focused on stiff priming and stiff-correlated mechanical memory because these conditions are the most widely studied because of applicability in stem cell therapies for fibrosis and osteogenesis. However, cells can also develop analogous soft-correlated mechanical memory, which can eventually lead to soft tissue generation such as neurogenesis with sufficient priming (1). Our model is instantly generalizable to this case by reconstructing x as an averaged quantity of soft-activated phenotype components ($\vec{x} \rightarrow \vec{x}_{stiff}$, \vec{x}_{soft}) and inverting the scaled stiffness from $\frac{m}{m_0}$ to $\frac{m_0}{m}$ (Fig. 7, a–c). The phase diagram for soft-correlated memory and phenotypic activation is shown in Fig. S6 and retains the three distinct regions that allow for no memory, temporary memory, and permanent memory depending on priming time. Recent experiments that primed adipose stem cells on 1 kPa substrates for 2 weeks found that temporary soft memory develops with similar persistence times (between 1 and 2 weeks) to stiff memory (10). In contrast with stiff priming, nuclear YAP localization was not found to be a marker of soft priming. This observation agrees well with our definition of the mechanically correlated phenotype fingerprint vector \vec{x} ; nuclear YAP is an element of the stiff-correlated \vec{x} , but not the softcorrelated \vec{x} . Using this simple, modular model framework, more complex models can be assembled that simultaneously consider soft and stiff memory and downstream consequences for differentiation.

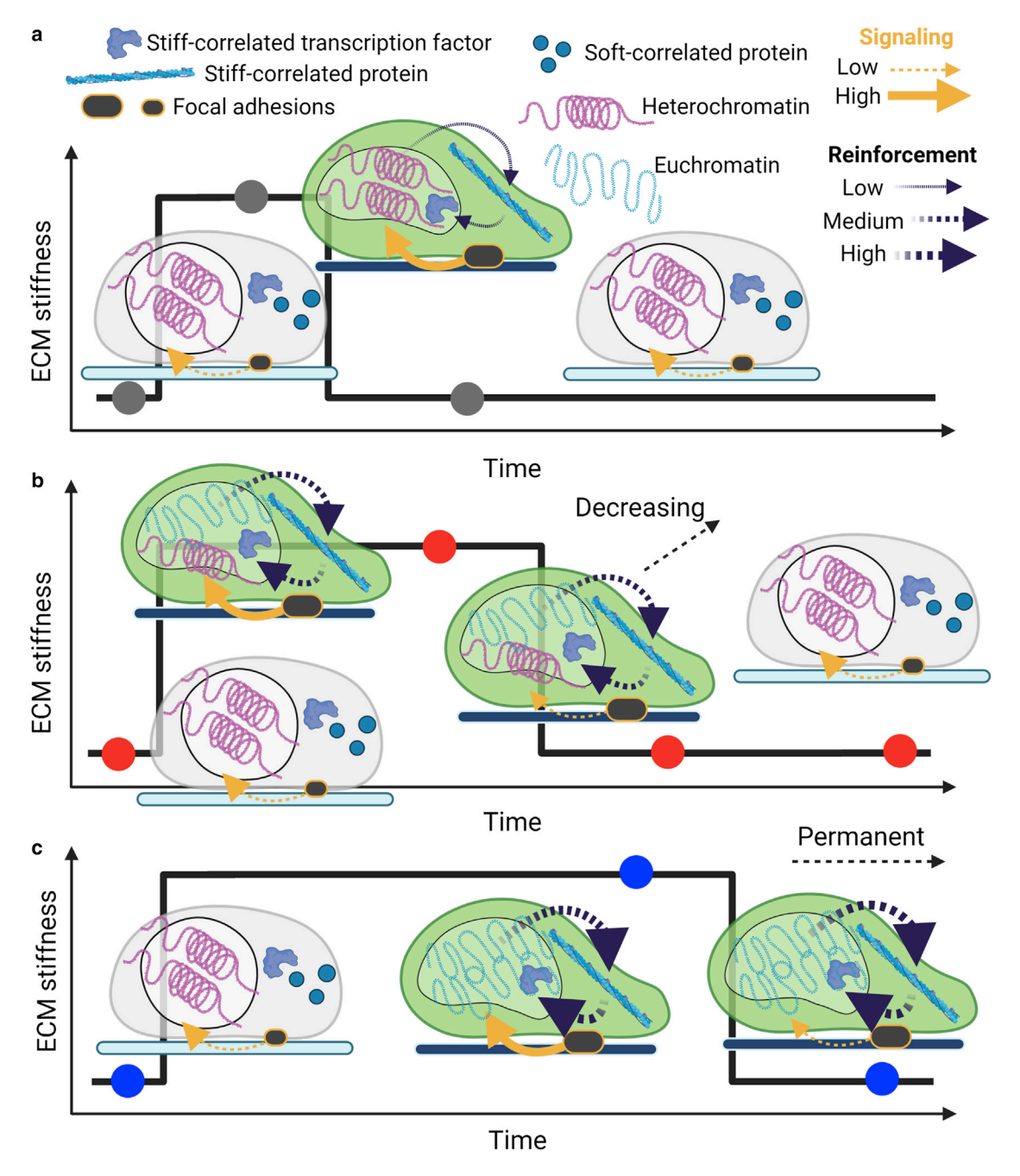


FIGURE 7 Summary of dynamic mechanical memory. (a) At short priming times, mechanical signaling leads to cellular adaptation but does not persist for sufficient time to increase reinforcement, leading to no memory. subsequent reinforcement is low, preventing observation of memory. (b) At intermediate priming times, reinforcement increases with persisting mechanical signal. The transcriptional environment shifts enough to build temporary memory, but this reinforcement will slowly decay to erase memory once the mechanical signal is removed. (c) At long priming times, reinforcement strength continues to grow with input mechanical signal and an adapting transcriptional environment. Reinforcement becomes strong enough to sustain without any mechanical signal, and the new phenotype persists if the substrate is changed (permanent memory). To see this figure in color, go online.

DISCUSSION

The acquisition and maintenance of mechanical memory is a general phenomenon across different cell types and culture environments (4–10,68). Balestrini et al. (4) cultured lung fibroblasts for 2 weeks on stiff (100 kPa, priming phase) substrates and found that they continued to express elevated

fibrotic activity after being transferred to soft substrates (5 kPa, dissipative phase) for at least 2 weeks. A follow-up study by Li et al. under similar conditions identified miR-21 as a necessary molecule for long-time memory maintenance, indicating the role of transcriptional efficiency in memory regulation (5). Some miRNAs can have

half-lives on the scale of multiple days, which motivated our formulation of $\alpha(t_{slow})$ to conceptually include these noncoding RNA molecules. More recent experiments have focused on detailed changes of chromatin organization within the nucleus, confirming that epigenetic changes occur in response to mechanical signaling (8) and highlighting the role of the LINC complex as a direct, physical mechanosensory (12,52,62). Additionally, we have recently shown that epithelial cell sheets primed on a stiff matrix for 3 days also store mechanical memory through nuclear YAP localization, which continues to enhance cell migration through enhanced pMLC expression and focal adhesion formation on soft matrix for 2-3 days (7).

In developing our model, we sought to synthesize and distill the phenomenological observations from these experiments and related studies covering the impact of mechanics on lineage specification, which has not been accomplished by existing models to our knowledge. Li et al. (5) proposed a reservoir model along with their identification of miR-21 as a memory regulator, in which priming leads to production of memory keepers that slowly dissipate after priming halts. This model alone does not explain the timescale disparity between mechanical adaptation and development of memory. Mousavi et al. (28) and Peng et al. (26) proposed two different mechanically activated differentiation models based on population dynamics and gene regulatory networks, but these models do not capture the variable rates of memory dissipation observed in experiments. These models rely on \sim 20 and \sim 40 free kinetic parameters, respectively, yet do not account for key qualitative features of the memory phenomena. Our model uses eight unique free parameters, which sacrifices resolution on specific biological mechanisms but allows us to identify that a simple nonlinear coupling between signaling and transcriptional evolution is sufficient to capture the phenomenological features of cellular plasticity.

The continuous range of cellular plasticity persistence time from zero (no memory, Fig. 7 a) to permanent (lineage specification, Fig. 7 c) is unique when compared to other physical memory systems, which often either exhibit permanent memory or no memory. Although early studies of lineage specification viewed this process as unidirectional (such as the traditional Waddington landscape), the targeted reversibility of plasticity under the right conditions is also a unique physical feature. The traditional Waddington landscape identifies specific branch points that split cells into separate wells representing stable phenotypes (24). Our model generalizes this picture by showing that both the Waddington landscape surface and the rate at which the cell progresses down each well can be altered by external stimuli such as stiffness. This "graduated reversibility" may function biologically to make the cell more resilient to local short-term fluctuations in environment while still allowing for long-term, correlated population shifts in response to persistent environmental cues.

Predicting the memory response of cells to their mechanical environment has significant implications for designing cell-based therapy and studying other cellular mechanisms in vitro. Based on our model, we predict that small changes in priming stiffness or priming time can have large consequences on the retention time of developed phenotypes due to the nonlinearity of slow-evolving components. Our phase diagram indicates that recovery of stem-like soft phenotypes can be enhanced after priming by reducing the stiffness of the recovery substrate, extending the range of region III that allows for memory dissipation. However, beyond a certain point, mechanical signal alone will not lead to phenotype reversal because of formation of permanent memory. Measuring the extent of priming may require nuclear information and not just data on signal activity, as the timescale of signaling is independent of the timescale of memory development. External methods to change α , such as Yamanaka factors or changes in growth media, can overwrite the natural permanent persistence of the stiff phenotype in these situations. In future work, we anticipate that this model framework for mechanical memory can be extended to include a chemical axis, which can be used to consider more general cases of cell differentiation and coupling between chemical and mechanical contributions to memory acquisition and retention.

Limitations

In our model, we made two key assumptions: 1) positive feedback loops exist in mechanosensing pathways and 2) shifts in the transcriptional environment that affect these feedback loops depend on signaling but occur on slow timescales. Quantitative predictions of cell responses will require more experimental data to validate more complex and precise models. Based on our results in this work, determining the rate of change of the transcriptional environment $(\alpha(t))$ as a function of priming stiffness and priming time is the most important unknown quantity. This is difficult to assess from epigenetic modifiers alone because chromatin reorganization occurs on a longer timescale than epigenetic enzyme activity. High throughput chromatin conformation capture (Hi-C) experiments during both priming and memory dissipation would provide information on the rate of change of the chromatin conformation. Although this would not completely specify the transcriptional environment, this information would be key to understand which steps are rate limiting in the evolution of mechanically activated cellular plasticity. The further that $\alpha(t)$ can be specified with mechanistic information from the nucleus, the greater predictive accuracy on the dynamics of memory can be.

SUPPORTING MATERIAL

Supporting material can be found online at https://doi.org/10.1016/j.bpj. 2021.10.006

AUTHOR CONTRIBUTIONS

Conceptualization: C.C.P., J.M., A.P., J.D.B., and V.B.S.; methodology: C.C.P., J.M., A.P., and V.B.S.; investigation: C.C.P. and J.M.; visualization: C.C.P. and J.M.; supervision: J.D.B., A.P., and V.B.S.; writing—original draft: C.C.P.; writing—review and editing: C.C.P., J.M., A.P., J.D.B., and V.B.S.

ACKNOWLEDGMENTS

This work was supported by National Cancer Institute awards R01CA232256 (V.B.S.) and U54CA261694 (V.B.S.), National Institute of Biomedical Imaging and Bioengineering awards R01EB017753 (V.B.S.) and R01EB030876 (V.B.S.), National Science Foundation Center for Engineering Mechanobiology grant CMMI-154857 (J.D.B., A.P., and V.B.S.), National Science Foundation grants MRSEC/DMR-1720530 (V.B.S.) and DMS-1953572 (V.B.S.), National Institute of Health/National Institute of General Medical Sciences award R35GM128764 (A.P.), and National Institute of Arthritis and Musculoskeletal and Skin Diseases grant 5R01AR073809 (J.B.).

SUPPORTING CITATIONS

References (69–71) appear in the Supporting material.

REFERENCES

- Engler, A. J., S. Sen, ..., D. E. Discher. 2006. Matrix elasticity directs stem cell lineage specification. *Cell*. 126:677–689.
- Schiller, H. B., and R. Fässler. 2013. Mechanosensitivity and compositional dynamics of cell-matrix adhesions. EMBO Rep. 14:509–519.
- Hynes, R. O. 2009. The extracellular matrix: not just pretty fibrils. Science, 326:1216–1219.
- Balestrini, J. L., S. Chaudhry, ..., B. Hinz. 2012. The mechanical memory of lung myofibroblasts. *Integr. Biol.* 4:410–421.
- Li, C. X., N. P. Talele, ..., B. Hinz. 2017. MicroRNA-21 preserves the fibrotic mechanical memory of mesenchymal stem cells. *Nat. Mater.* 16:379–389.
- Yang, C., M. W. Tibbitt, ..., K. S. Anseth. 2014. Mechanical memory and dosing influence stem cell fate. *Nat. Mater.* 13:645–652.
- Nasrollahi, S., C. Walter, ..., A. Pathak. 2017. Past matrix stiffness primes epithelial cells and regulates their future collective migration through a mechanical memory. *Biomaterials*. 146:146–155.
- Killaars, A. R., J. C. Grim, ..., K. S. Anseth. 2018. Extended exposure to stiff microenvironments leads to persistent chromatin remodeling in human mesenchymal stem cells. Adv. Sci. (Weinh.). 6:1801483.
- Watson, A. W., A. D. Grant, ..., G. Mouneimne. 2021. Breast tumor stiffness instructs bone metastasis via maintenance of mechanical conditioning. *Cell Rep.* 35:109293.
- Dunham, C., N. Havlioglu, ..., G. Meyer. 2020. Adipose stem cells exhibit mechanical memory and reduce fibrotic contracture in a rat elbow injury model. FASEB J. 34:12976–12990.
- Uhler, C., and G. V. Shivashankar. 2017. Regulation of genome organization and gene expression by nuclear mechanotransduction. *Nat. Rev. Mol. Cell Biol.* 18:717–727.
- Nemec, S., and K. A. Kilian. 2021. Materials control of the epigenetics underlying cell plasticity. *Nat. Rev. Mater.* 6:69–83.
- Hammer, D. A., and D. A. Lauffenburger. 1987. A dynamical model for receptor-mediated cell adhesion to surfaces. *Biophys. J.* 52:475–487.
- Choquet, D., D. P. Felsenfeld, and M. P. Sheetz. 1997. Extracellular matrix rigidity causes strengthening of integrin-cytoskeleton linkages. *Cell*. 88:39–48.

- Chrzanowska-Wodnicka, M., and K. Burridge. 1996. Rho-stimulated contractility drives the formation of stress fibers and focal adhesions. J. Cell Biol. 133:1403–1415.
- Olson, E. N., and A. Nordheim. 2010. Linking actin dynamics and gene transcription to drive cellular motile functions. *Nat. Rev. Mol. Cell Biol.* 11:353–365.
- Doss, B. L., M. Pan, ..., B. Ladoux. 2020. Cell response to substrate rigidity is regulated by active and passive cytoskeletal stress. *Proc. Natl. Acad. Sci. USA*. 117:12817–12825.
- Discher, D. E., P. Janmey, and Y. L. Wang. 2005. Tissue cells feel and respond to the stiffness of their substrate. Science. 310:1139–1143.
- Dupont, S., L. Morsut, ..., S. Piccolo. 2011. Role of YAP/TAZ in mechanotransduction. *Nature*. 474:179–183.
- Fearing, B. V., L. Jing, ..., L. A. Setton. 2019. Mechanosensitive transcriptional coactivators MRTF-A and YAP/TAZ regulate nucleus pulposus cell phenotype through cell shape. FASEB J. 33:14022–14035.
- Makhija, E., D. S. Jokhun, and G. V. Shivashankar. 2016. Nuclear deformability and telomere dynamics are regulated by cell geometric constraints. *Proc. Natl. Acad. Sci. USA*. 113:E32–E40.
- Jain, N., K. V. Iyer, ..., G. V. Shivashankar. 2013. Cell geometric constraints induce modular gene-expression patterns via redistribution of HDAC3 regulated by actomyosin contractility. *Proc. Natl. Acad. Sci. USA*. 110:11349–11354.
- Heo, S. J., S. D. Thorpe, ..., R. L. Mauck. 2015. Biophysical regulation of chromatin architecture instills a mechanical memory in mesenchymal stem cells. Sci. Rep. 5:16895.
- Ferrell, J. E., Jr. 2012. Bistability, bifurcations, and Waddington's epigenetic landscape. *Curr. Biol.* 22:R458–R466.
- Huang, S. 2012. The molecular and mathematical basis of Waddington's epigenetic landscape: a framework for post-Darwinian biology? *BioEssays*. 34:149–157.
- Peng, T., L. Liu, ..., Q. Nie. 2017. A mathematical model of mechanotransduction reveals how mechanical memory regulates mesenchymal stem cell fate decisions. *BMC Syst. Biol.* 11:55.
- Ascolani, G., T. M. Skerry, ..., A. Shuaib. 2020. Revealing hidden information in osteoblast's mechanotransduction through analysis of time patterns of critical events. *BMC Bioinformatics*. 21:114.
- Mousavi, S. J., and M. H. Doweidar. 2015. Role of mechanical cues in cell differentiation and proliferation: a 3D numerical model. *PLoS One*. 10:e0124529.
- Kwon, Y.-K., and K.-H. Cho. 2008. Coherent coupling of feedback loops: a design principle of cell signaling networks. *Bioinformatics*. 24:1926–1932.
- Tsai, T. Y. C., Y. S. Choi, ..., J. E. Ferrell, Jr. 2008. Robust, tunable biological oscillations from interlinked positive and negative feedback loops. *Science*. 321:126–129.
- Mitarai, N., M. H. Jensen, and S. Semsey. 2015. Coupled positive and negative feedbacks produce diverse gene expression patterns in colonies. MBio. 6:e00059-15.
- Kwon, Y.-K., and K.-H. Cho. 2008. Quantitative analysis of robustness and fragility in biological networks based on feedback dynamics. *Bio-informatics*. 24:987–994.
- 33. Mitra, T., S. N. Menon, and S. Sinha. 2018. Emergent memory in cell signaling: persistent adaptive dynamics in cascades can arise from the diversity of relaxation time-scales. *Sci. Rep.* 8:13230.
- **34.** Shuaib, A., D. Motan, ..., D. Lacroix. 2019. Heterogeneity in the mechanical properties of integrins determines mechanotransduction dynamics in bone osteoblasts. *Sci. Rep.* 9:13113.
- Halder, G., S. Dupont, and S. Piccolo. 2012. Transduction of mechanical and cytoskeletal cues by YAP and TAZ. *Nat. Rev. Mol. Cell Biol.* 13:591–600.
- 36. Elosegui-Artola, A., I. Andreu, ..., P. Roca-Cusachs. 2017. Force triggers YAP nuclear entry by regulating transport across nuclear pores. *Cell.* 171:1397–1410.e14.

- 37. Zonderland, J., S. Rezzola, and L. Moroni. 2020. Actomyosin and the MRTF-SRF pathway downregulate FGFR1 in mesenchymal stromal cells. Commun. Biol. 3:576.
- 38. Kanno, T., T. Takahashi, ..., T. Nishihara. 2007. Mechanical stressmediated Runx2 activation is dependent on Ras/ERK1/2 MAPK signaling in osteoblasts. J. Cell. Biochem. 101:1266-1277.
- 39. Iyer, K. V., S. Pulford, ..., G. V. Shivashankar. 2012. Mechanical activation of cells induces chromatin remodeling preceding MKL nuclear transport. Biophys. J. 103:1416-1428.
- 40. Mullen, C. A., T. J. Vaughan, ..., L. M. McNamara. 2015. The effect of substrate stiffness, thickness, and cross-linking density on osteogenic cell behavior. Biophys. J. 108:1604-1612.
- 41. Nardone, G., J. Oliver-De La Cruz, ..., G. Forte. 2017. YAP regulates cell mechanics by controlling focal adhesion assembly. Nat. Commun.
- 42. Yu, O. M., J. A. Benitez, ..., J. H. Brown. 2018. YAP and MRTF-A, transcriptional co-activators of RhoA-mediated gene expression, are critical for glioblastoma tumorigenicity. Oncogene. 37:5492–5507.
- 43. Ege, N., A. M. Dowbaj, ..., E. Sahai. 2018. Quantitative analysis reveals that actin and src-family kinases regulate nuclear YAP1 and its export. Cell Syst. 6:692-708.e13.
- 44. Xiong, W., and J. E. Ferrell, Jr. 2003. A positive-feedback-based bistable 'memory module' that governs a cell fate decision. Nature. 426:460–465.
- 45. Mitrophanov, A. Y., and E. A. Groisman. 2008. Positive feedback in cellular control systems. BioEssays. 30:542-555.
- 46. Wang, L., B. L. Walker, ..., W. T. Tse. 2009. Bistable switches control memory and plasticity in cellular differentiation. Proc. Natl. Acad. Sci. USA. 106:6638-6643.
- 47. Young, D. W., M. Q. Hassan, ..., G. S. Stein. 2007. Mitotic retention of gene expression patterns by the cell fate-determining transcription factor Runx2. Proc. Natl. Acad. Sci. USA. 104:3189–3194.
- 48. Schroeder, T. M., E. D. Jensen, and J. J. Westendorf. 2005. Runx2: a master organizer of gene transcription in developing and maturing osteoblasts. Birth Defects Res. C Embryo Today. 75:213-225.
- 49. Calvo, F., N. Ege, ..., E. Sahai. 2013. Mechanotransduction and YAPdependent matrix remodelling is required for the generation and maintenance of cancer-associated fibroblasts. Nat. Cell Biol. 15:637-646.
- 50. Kegelman, C. D., J. M. Collins, ..., J. D. Boerckel. 2020. Gone caving: roles of the transcriptional regulators YAP and TAZ in skeletal development. Curr. Osteoporos. Rep. 18:526-540.
- 51. Heo, S. J., W. M. Han, ..., R. L. Mauck. 2016. Mechanically induced chromatin condensation requires cellular contractility in mesenchymal stem cells. Biophys. J. 111:864-874.
- 52. Walker, C. J., C. Crocini, ..., K. S. Anseth. 2021. Nuclear mechanosensing drives chromatin remodelling in persistently activated fibroblasts. Nat. Biomed. Eng 1-15, Published online April 19, 2021.
- 53. Bouzid, T., E. Kim, ..., J. Y. Lim. 2019. The LINC complex, mechanotransduction, and mesenchymal stem cell function and fate. J. Biol. Eng. 13:68.

- 54. Swift, J., I. L. Ivanovska, ..., D. E. Discher. 2013. Nuclear lamin-A scales with tissue stiffness and enhances matrix-directed differentiation. Science. 341:1240104.
- 55. Foster, C. T., F. Gualdrini, and R. Treisman. 2017. Mutual dependence of the MRTF-SRF and YAP-TEAD pathways in cancer-associated fibroblasts is indirect and mediated by cytoskeletal dynamics. Genes Dev. 31:2361-2375.
- 56. Kim, T., D. Hwang, ..., D. S. Lim. 2017. MRTF potentiates TEAD-YAP transcriptional activity causing metastasis. EMBO J. 36:520-535.
- 57. Meng, G., J. Wei, Y. Wang, D. Qu, and J. Zhang. 2020. MiR-21 regulates immunosuppression mediated by myeloid-derived suppressor cells by impairing RUNX1-YAP interaction in lung cancer. Cancer Cell Int. 20:495.
- 58. Qiao, Y., J. Chen, ..., M. Sudol. 2017. YAP regulates actin dynamics through ARHGAP29 and promotes metastasis. Cell Rep. 19:1495-
- 59. Shi, G., L. Liu, ..., D. Thirumalai. 2018. Interphase human chromosome exhibits out of equilibrium glassy dynamics. Nat. Commun. 9:3161.
- 60. Sardo, L., A. Lin, ..., Z. A. Klase. 2017. Real-time visualization of chromatin modification in isolated nuclei. J. Cell Sci. 130:2926–2940.
- 61. Gantier, M. P., C. E. McCoy, ..., B. R. G. Williams. 2011. Analysis of microRNA turnover in mammalian cells following Dicer1 ablation. Nucleic Acids Res. 39:5692-5703.
- 62. Killaars, A. R., C. J. Walker, and K. S. Anseth. 2020. Nuclear mechanosensing controls MSC osteogenic potential through HDAC epigenetic remodeling. Proc. Natl. Acad. Sci. USA. 117:21258-21266.
- 63. Rabineau, M., F. Flick, ..., D. Vautier. 2018. Chromatin de-condensation by switching substrate elasticity. Sci. Rep. 8:12655.
- 64. Passaro, F., I. De Martino, ..., T. Russo. 2021. YAP contributes to DNA methylation remodeling upon mouse embryonic stem cell differentiation. J. Biol. Chem. 296:100138.
- 65. Das, R. K., V. Gocheva, ..., A. E. Rowan. 2016. Stress-stiffening-mediated stem-cell commitment switch in soft responsive hydrogels. Nat. Mater. 15:318-325.
- 66. Cui, Y., F. M. Hameed, ..., M. Sheetz. 2015. Cyclic stretching of soft substrates induces spreading and growth. Nat. Commun. 6:6333.
- 67. Takahashi, K., and S. Yamanaka. 2006. Induction of pluripotent stem cells from mouse embryonic and adult fibroblast cultures by defined factors. Cell. 126:663-676.
- 68. Yang, C., F. W. DelRio, ..., K. S. Anseth. 2016. Spatially patterned matrix elasticity directs stem cell fate. Proc. Natl. Acad. Sci. USA. 113:E4439-E4445.
- 69. Cosgrove, B. D., C. Loebel, ..., R. L. Mauck. 2021. Nuclear envelope wrinkling predicts mesenchymal progenitor cell mechano-response in 2D and 3D microenvironments. Biomaterials. 270:120662.
- 70. Jacob, F., and J. Monod. 1961. Genetic regulatory mechanisms in the synthesis of proteins. J. Mol. Biol. 3:318–356.
- 71. Maniatis, T., and R. Reed. 2002. An extensive network of coupling among gene expression machines. Nature. 416:499-506.

Biophysical Journal, Volume 120

Supplemental information

Dynamic self-reinforcement of gene expression determines acquisition of cellular mechanical memory

Christopher C. Price, Jairaj Mathur, Joel D. Boerckel, Amit Pathak, and Vivek B. Shenoy

Supplementary Materials for

Dynamic Self-Reinforcement of Gene Expression Determines Acquisition of Cellular Mechanical Memory

Christopher C. Price, 1,2,† Jairaj Mathur, 2,3,† Joel D. Boerckel, 2,4,5 Amit Pathak, 2,3,* Vivek B. Shenoy 1,2,*

This PDF file includes:

Supplementary Text Table S1 Figs. S1 to S6 Supporting References

¹ Department of Materials Science and Engineering, University of Pennsylvania, Philadelphia, PA 19104, USA.

² Center for Engineering Mechanobiology, University of Pennsylvania, Philadelphia, PA 19104, USA

³ Department of Mechanical Engineering & Materials Science, Washington University, St. Louis, MO, USA

⁴ Department of Orthopaedic Surgery, Perelman School of Medicine, University of Pennsylvania, Philadelphia, PA, USA.

⁵ Department of Bioengineering, University of Pennsylvania, Philadelphia, PA 19104, USA.

^{*} Corresponding Authors. Email: vshenoy@seas.upenn.edu; pathaka@wustl.edu

[†] These authors contributed equally to this work.

Supplementary Text

Section I: Generalized Model for Dynamic Self-Reinforcing Mechanosensitivity

Consider a vector variable \vec{x} where elements $x_{i=1..n}$ represent functionally active concentrations of stiff-activated proteins and transcription factors. For a cytoskeletal protein, x_i corresponds to the steady-state concentration which emerges from synthesis and degradation. Examples of stiff-correlated cytoskeletal proteins include F-actin (or α -SMA), vinculin, and integrins. For transcription factors, x_i refers to a transcriptionally eligible concentration, which includes the steady-state level of nuclear localization. Examples of transcription factors with well-known stiff-correlated nuclear localization include YAP (1, 2), MKL-1 (3, 4), and RUNX2 (5, 6); nuclear localization is necessary for transcription factor activity due to the possibility of coactivation requirements. Enzymes which modify the epigenome such as HDAC and HAT are also included as elements of \vec{x} , as epigenetic changes demonstrate mechanosensitive activity patterns and alter chromatin organization (7). \vec{x} is a fingerprint state vector for the mechanical phenotype of the cell. For each element of \vec{x} , we can write a linear steady-state rate equation

$$\dot{x}_i = k_{\uparrow i}(m) \left(x_i^{ref} - x_i \right) - k_{\downarrow i}(m) x_i + \sum_i c_{ij}(m) x_i x_j \tag{s1}$$

where $\dot{x}_i = \frac{dx_i}{dt}$, m is the ECM stiffness, $k_{\uparrow i}(m)$ is the stiffness-dependent rate of nuclear import or protein synthesis for component i, and $k_{\downarrow i}(m)$ is the stiffness-dependent rate of nuclear export or protein degradation for component i. $\overrightarrow{x^{ref}}$ with elements $x_{i=1..n}^{ref}$ is a vector of arbitrary reference concentrations such that the steady-state concentration $x_i = x_i^{ref}$ when stiffness $m = m_0$. c_{ij} are elements of the cooperativity matrix C which we define to be the matrix of activity coefficients which describe the degree of cooperation or anti-cooperation between different elements of \vec{x} . Additional cooperativity matrices corresponding to more complex interactions between elements of \vec{x} can be defined and added to Eq. s1. This defines a coupled set of rate equations for each mechanosensitive phenotype marker of the cell which has a unique steady state depending on the value of m.

Next, we consider contributions from positive feedback loops to the dynamics of each element of \vec{x} . Positive feedback loops arise from active transcription which assists phenotypic shifts that promote further transcription. We add a Hill relation with coefficient β to each equation for \vec{x}_l

$$\dot{x}_i = k_{\uparrow i}(m) \left(x_i^{ref} - x_i \right) - k_{\downarrow i}(m) x_i + \sum_j c_{ij}(m) x_i x_j + \alpha_i (\overrightarrow{y_k}, z) \frac{x_i^{\beta}}{x_i^{\beta} + 1}$$
 (s2)

scaled by sensitivity $\alpha_i(\overrightarrow{y_k}, z)$, which are components of the sensitivity vector $\overrightarrow{\alpha}$. $\overrightarrow{y_k}$ is a vector of concentrations of global transcriptional participants, which may or may not all be explicitly mechanosensitive; $\overrightarrow{y_k}$ contains all the components of \overrightarrow{x} , and therefore has dependence on ECM stiffness m. z is a label of the chromatin conformational state, which can be thought of as the single-cell Hi-C map of chromatin contacts; z also depends on m via physical changes to the nucleus initiated by the LINC complex (8, 9). Altogether, the chromatin state z and the global transcriptional cofactors $\overrightarrow{y_k}$ determine how effectively the mechanosensitive components of \overrightarrow{x} can self-reinforce.

Section II: Derivation of Nonlinearly Dynamic Reinforcement Sensitivity

Each element $\alpha_i(\overrightarrow{y_k}, z)$ can be written as a sum expansion of reinforcement matrices $A^{(n)}$ multiplying $\overrightarrow{y_k}$ and z:

$$\alpha_{i} = \sum_{k} a_{ik}^{(1)} y_{k} + a_{iz}^{(1)} z + \sum_{k} a_{ikz}^{(2)} y_{k} z + \sum_{k,l} a_{ikl}^{(2)} y_{k} y_{l} + \sum_{k,l} a_{iklz}^{(3)} y_{k} y_{l} z \dots$$
 (s3)

where a^n are elements of reinforcement matrices A^n with dimension n+1. These matrix elements are weights which represent the degree to which each component of the global transcriptional environment or the global chromatin conformational state influences the self-reinforcing capability of mechanosensitive component x_i . The weights are analogous to activity coefficients in regular solution theory, where cooperativity between different species in solution can cause nonlinear thermodynamics of mixing far from the dilute limit. This cooperativity arises from favorable binding interactions between solute species and long-range forces in polar media. These same features are prominent in the nucleoplasm, particularly the catalysis of transcription by formation of multi-component binding complexes (10, 11).

We are interested in how this self-reinforcing capability evolves over time, and using the chain rule we can write the time derivative of α_i as

$$\frac{d\alpha_i}{dt} = \sum_{k} \frac{\partial \alpha_i}{\partial y_k} \frac{\partial y_k}{\partial t} + \frac{\partial \alpha_i}{\partial z} \frac{\partial z}{\partial t}$$
 (s4)

Plugging Eq. s3 into Eq. s4, we arrive at

$$\frac{d\alpha_{i}}{dt} = \sum_{k,l...} (a_{ik}^{(1)} + a_{ikz}^{(2)}z + a_{ikl}^{(2)}y_{l} + a_{iklz}^{(3)}y_{l}z + ...) \frac{\partial y_{k}}{\partial t} + (a_{iz}^{(1)} + a_{ikz}^{(2)}y_{k} + ...) \frac{\partial z}{\partial t}$$
(s5)

Here, we see that the dynamics of self-reinforcement sensitivity depend on dynamics of the transcription regulatory environment and the chromatin conformation, weighted by the matrix elements of the reinforcement matrices $A_i^{(n)}$. $\frac{dy_k}{dt}$ and $\frac{dz}{dt}$ are equivalent to timescales τ for each transcriptionally active component and the chromatin conformation, respectively, and generally can depend on x_i and m. The coefficients a_{ik}^n are generally non-linear functions of y_k , analogously for $a_{zk}^{(n)}$ depending on z. Given sufficient data to populate the partial derivative relations and reinforcement matrices in Eq. s5, the steady-state dynamics of cellular plasticity can be completely specified through this framework. However, this relies on highly detailed, time-dependent mechanistic knowledge which is far beyond the scope of current experimental or simulation techniques. Rather than estimate all these individual relationships with placeholder coefficients or linear rate equations, we separate the components of Eq. s5 into two timescales and perform an averaging to distill out complexity while preserving phenomenological features. Since the vector y_k contains transcriptionally active components of x and therefore depends on the mechanical priming program m(t), we know that some terms in Eq. s5 will change on the same timescale as x_i and that this timescale is an upper bound for $\frac{d\alpha_i}{dt}$. We make an arbitrary but phenomenologically justified choice of $\overrightarrow{c_i} \frac{m^{\zeta}}{m^{\zeta+1}}$ to represent these fast non-linear processes, where the time dependence originates from m(t), and gather the slower terms into a separate term $\alpha_i(t_{slow})$. This term still retains x_i dependence and m dependence from components of $\frac{dy_k}{dt}$ and $\frac{dz}{dt}$ but contains all the slower processes in these vectors (introduced as $\tau_s \frac{m}{m_0}$ and τ_f) as well as the nonlinear scaling originating

from the coefficients of $A_i^{(n)}$ (introduced as $\alpha \exp(-\frac{x}{x_{ref}})$). Splitting $\alpha_i(t_{slow})$ into a piecewise function by region is a phenomenological choice but reflects the fact that different terms favoring an increase, decrease, or equilibration of the sensitivity will dominate depending on the magnitude of the external mechanical signal. Finally, when we perform an averaging over the components x_i in the main text, the system of equations described in Eq. s5 collapse into a single equation below with two terms in each region describing both fast and slow dynamics of mechanosensitive self-reinforcement.

$$\frac{d\alpha}{dt} = \begin{cases}
-\frac{\alpha - \alpha_0}{\tau_f} + c \frac{m^{\zeta}}{m^{\zeta} + 1}, & I \\
\frac{\alpha}{\tau_s} \frac{m}{m_0} \exp{-\frac{x}{x_{ref}}} + c \frac{m^{\zeta}}{m^{\zeta} + 1}, & II \\
-\frac{\alpha}{\tau_s} \frac{m}{m_0} \exp{-\frac{x}{x_{ref}}} + c \frac{m^{\zeta}}{m^{\zeta} + 1}, & III
\end{cases} \tag{s6}$$

Section III: Linear Dynamics used for Noise Simulations

Linear Dynamics for
$$\frac{d\alpha}{dt_{slow}}$$
 (Figure S5):

$$\frac{d\alpha}{dt_{slow}} = \begin{cases} -\frac{\alpha - \alpha_0}{\tau_f}, & I\\ \frac{\alpha}{\tau_s}, & II\\ -\frac{\alpha}{\tau_s}, & III \end{cases}$$

Reference	Cell Type	Priming Stiffness (kPa)	Priming Time (days)	Memory Stiffness (kPa)	Memory Time (days)	Memory marker
Yang et al. (12)	hMSC	10	1, 7, 10	2	1, 5+, 10+	YAP, RUNX2
Balestrini et al. (13)	Fibroblasts	25, 100	14	5	14+	α-SMA
Xi et al. (14)	rMSC	100	21	5	14+	α-SMA, miR- 21
Nasrollahi et al. (15)	mcf10a A431 Mcf7	50	3	0.5	3+	pMLC, YAP, migration speed
Watson et al. (16)	SUM159	8	7	0.5	2 to 7	RUNX2, migration speed
Dunham et al. (17)	ASC	5	14	100	7 to 14	Cell area, α- SMA

Table S1. Summary of experimental data collected on mechanical memory.

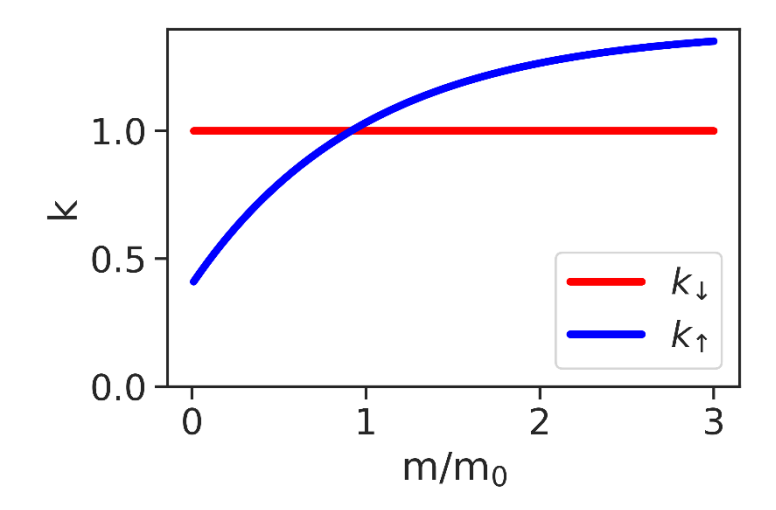


Fig. S1.Mechanosensitivity of synthesis and nuclear localization of stiff-correlated transcription factors (blue) and countering degradation and nuclear export (red).

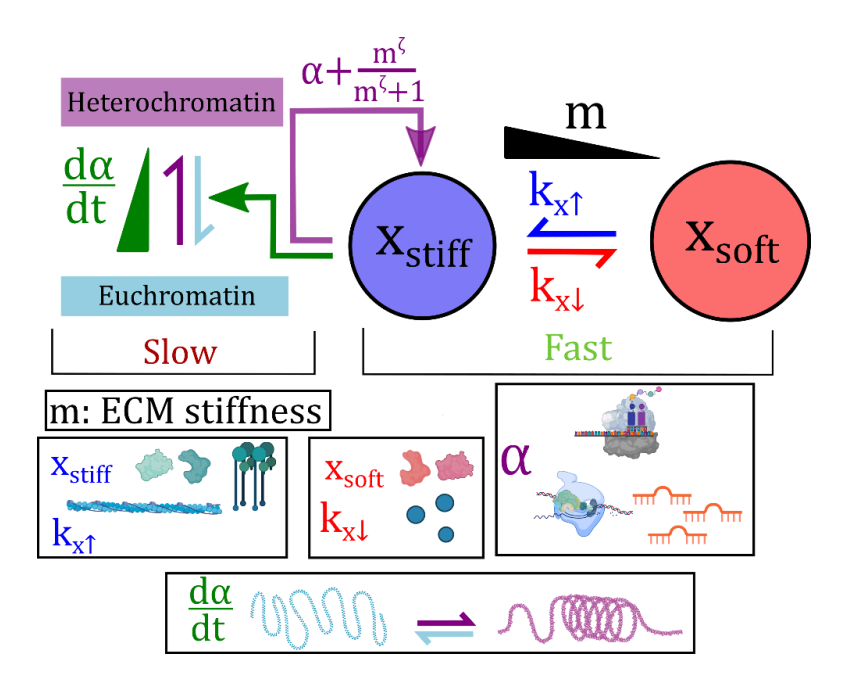


Fig. S2.

Circuit diagram of the dynamic mechanical memory model. x represents the mechanoactivated phenotype of the cell including nuclear localized transcription factors such as YAP, RUNX2, and MKL-1. m represents ECM stiffness. Nuclear x self-reinforces with transcriptional efficiency $\alpha + \frac{m^{\zeta}}{m^{\zeta}+1}$; the first term represents signal-driven effects on transcription, while the second term represents LINC-driven physical processes. $\frac{d\alpha}{dt}$ gives the change of the efficiency of this self-reinforcement over time *via* a modified transcriptional landscape.

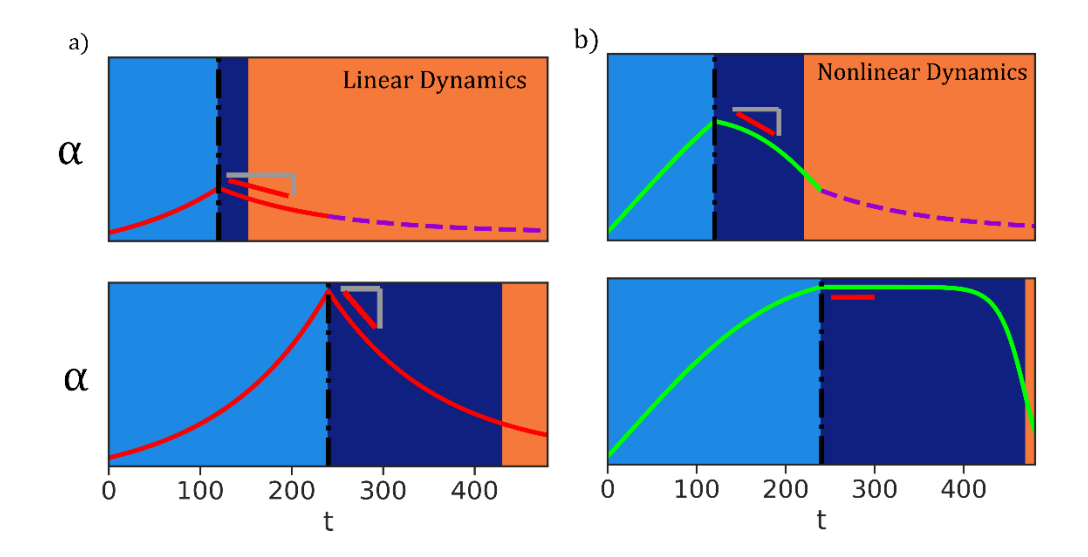


Fig. S3. Comparison of linear and non-linear dynamics of α . (A) Linear dynamics. (B) Nonlinear dynamics. While shorter primes (top row) lead to less memory (width of dark blue region) than longer primes (bottom row) for both (A) and (B), the initial rate of memory dissipation is much faster in (A) than in (B); (B) matches better with experiment.

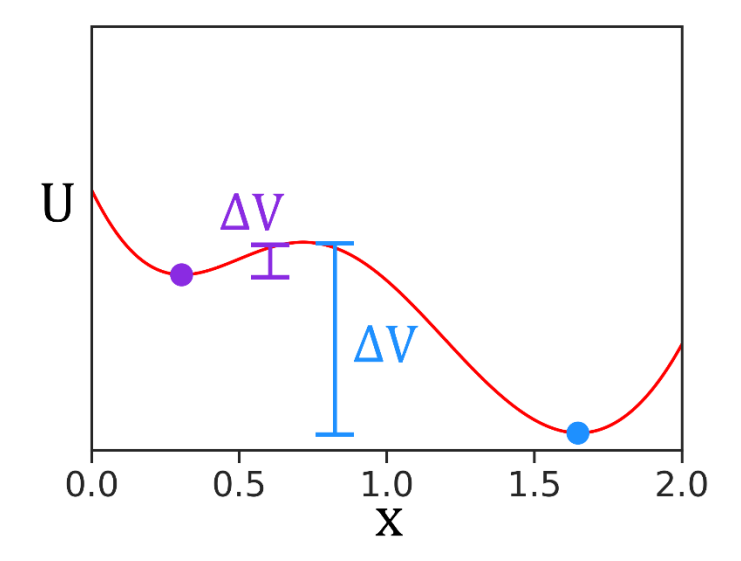


Fig. S4.Illustration of local minima in region III of the phase diagram shown in Figure 2. If random fluctuations perturb the state from the steady state minimum, the population in the shallow well (purple) will be reduced relative to the population in the deeper well (blue).

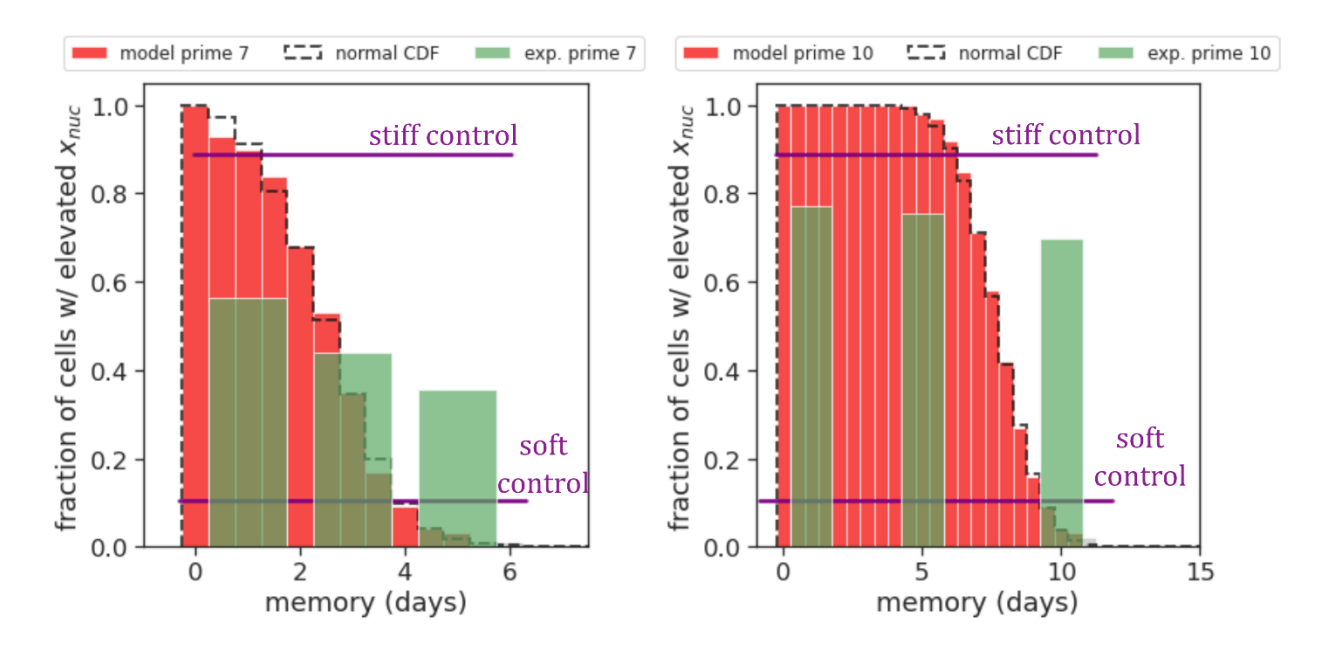


Fig. S5.

Noise study with linear dynamics, where dependence of the slow varying component of $\frac{d\alpha}{dt}$ on x is removed. Gaussian noise applied in this situation leads to a normal distribution of memory time, in contrast with the non-normal distribution of nonlinear dynamics and in contrast with experimental results (green bars).

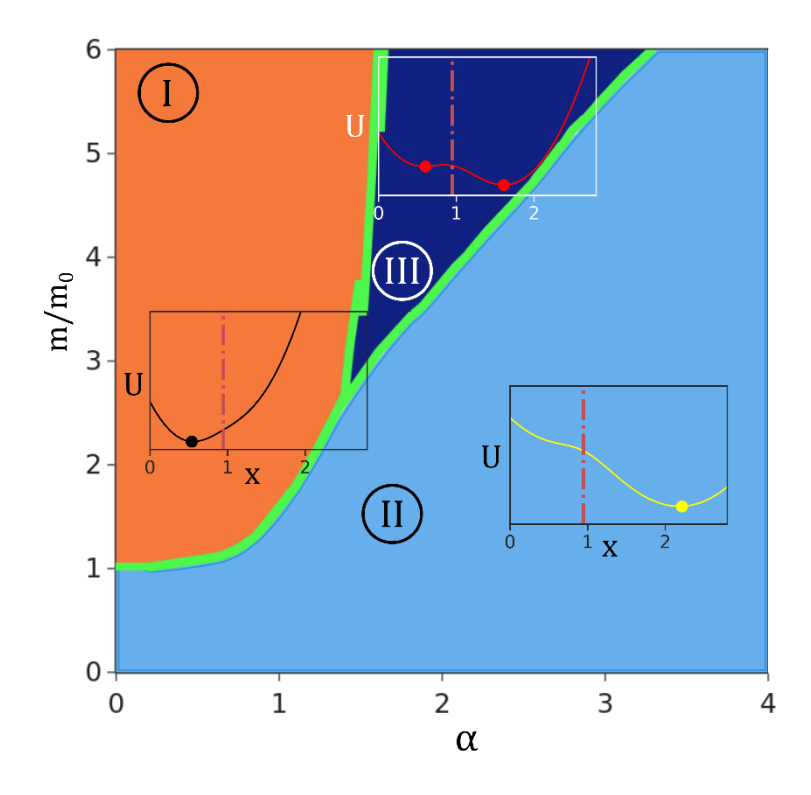


Fig. S6. Analogous phase diagram of the model for soft-activated genes. In the model, the mechanoactivation profile / mechanical signaling is reversed by flipping $\frac{m}{m_0}$ to $\frac{m_0}{m}$, so that $\frac{dx}{dt}$ increases when stiffness is reduce. In this case, high x corresponds to activity of soft-correlated phenotypic genes and transcription factors. α now represents positive reinforcement for gene expression correlating with a soft phenotype.

Supporting References

- 1. G. Halder, S. Dupont, S. Piccolo, Transduction of mechanical and cytoskeletal cues by YAP and TAZ. *Nat. Rev. Mol. Cell Biol.* **13**, 591–600 (2012).
- 2. A. Elosegui-Artola, I. Andreu, A. E. M. Beedle, A. Lezamiz, M. Uroz, A. J. Kosmalska, R. Oria, J. Z. Kechagia, P. Rico-Lastres, A. L. Le Roux, C. M. Shanahan, X. Trepat, D. Navajas, S. Garcia-Manyes, P. Roca-Cusachs, Force Triggers YAP Nuclear Entry by Regulating Transport across Nuclear Pores. *Cell.* 171, 1397-1410.e14 (2017).
- 3. B. V. Fearing, L. Jing, M. N. Barcellona, S. E. Witte, J. M. Buchowski, L. P. Zebala, M. P. Kelly, S. Luhmann, M. C. Gupta, A. Pathak, L. A. Setton, Mechanosensitive transcriptional coactivators MRTF-A and YAP/TAZ regulate nucleus pulposus cell phenotype through cell shape. *FASEB J.* **33**, 14022–14035 (2019).
- 4. J. Zonderland, S. Rezzola, L. Moroni, Actomyosin and the MRTF-SRF pathway downregulate FGFR1 in mesenchymal stromal cells. *Commun. Biol.* **3**, 1–11 (2020).
- 5. T. Kanno, T. Takahashi, T. Tsujisawa, W. Ariyoshi, T. Nishihara, Mechanical stress-mediated Runx2 activation is dependent on Ras/ERK1/2 MAPK signaling in osteoblasts.

- J. Cell. Biochem. 101, 1266–1277 (2007).
- 6. K. V. Iyer, S. Pulford, A. Mogilner, G. V. Shivashankar, Mechanical activation of cells induces chromatin remodeling preceding MKL nuclear transport. *Biophys. J.* **103**, 1416–1428 (2012).
- 7. A. R. Killaars, J. C. Grim, C. J. Walker, E. A. Hushka, T. E. Brown, K. S. Anseth, Extended Exposure to Stiff Microenvironments Leads to Persistent Chromatin Remodeling in Human Mesenchymal Stem Cells. *Adv. Sci.* **6**, 1801483 (2019).
- 8. T. Bouzid, E. Kim, B. D. Riehl, A. M. Esfahani, J. Rosenbohm, R. Yang, B. Duan, J. Y. Lim, The LINC complex, mechanotransduction, and mesenchymal stem cell function and fate. *J. Biol. Eng.* **13**, 68 (2019).
- 9. B. D. Cosgrove, C. Loebel, T. P. Driscoll, T. K. Tsinman, E. N. Dai, S. J. Heo, N. A. Dyment, J. A. Burdick, R. L. Mauck, Nuclear envelope wrinkling predicts mesenchymal progenitor cell mechano-response in 2D and 3D microenvironments. *Biomaterials*. **270**, 120662 (2021).
- 10. F. Jacob, J. Monod, Genetic regulatory mechanisms in the synthesis of proteins. *J. Mol. Biol.* **3** (1961), pp. 318–356.
- 11. T. Maniatis, R. Reed, An extensive network of coupling among gene expression machines. *Nature*. **416**, 499–506 (2002).
- 12. C. Yang, M. W. Tibbitt, L. Basta, K. S. Anseth, Mechanical memory and dosing influence stem cell fate. *Nat. Mater.* **13**, 645–652 (2014).
- 13. J. L. Balestrini, S. Chaudhry, V. Sarrazy, A. Koehler, B. Hinz, The mechanical memory of lung myofibroblasts. *Integr. Biol.* **4**, 410 (2012).
- 14. C. X. Li, N. P. Talele, S. Boo, A. Koehler, E. Knee-Walden, J. L. Balestrini, P. Speight, A. Kapus, B. Hinz, MicroRNA-21 preserves the fibrotic mechanical memory of mesenchymal stem cells. *Nat. Mater.* **16**, 379–389 (2017).
- 15. S. Nasrollahi, C. Walter, A. J. Loza, G. V. Schimizzi, G. D. Longmore, A. Pathak, Past matrix stiffness primes epithelial cells and regulates their future collective migration through a mechanical memory. *Biomaterials.* **146**, 146–155 (2017).
- A. W. Watson, A. D. Grant, S. S. Parker, M. W. Harman, M. R. Roman, B. L. Uhlorn, C. Gowan, R. Castro-Portuguez, L. K. Stolze, C. Franck, D. A. Cusanovich, M. Padi, C. E. Romanoski, G. Mouneimne, Breast Tumor Stiffness Instructs Bone Metastasis Via Mechanical Memory. *Cell Rep.* 35, 109293 (2021).
- 17. C. Dunham, N. Havlioglu, A. Chamberlain, S. Lake, G. Meyer, Adipose stem cells exhibit mechanical memory and reduce fibrotic contracture in a rat elbow injury model. *FASEB J.* **34**, 12976–12990 (2020).